

Computational insights into the lipid code of transient receptor potential vanilloid channels reveal overlap with drug binding sites

Mario Lopez-Martin ^{a,b,1} , Eric Catalina-Hernandez ^{a,b,1} , Alex Peralvarez-Marín ^{a,b,*}

^a Unit of Biophysics, Department of Biochemistry and Molecular Biology, Facultat de Medicina, Av. Can Domènec s/n, Universitat Autònoma de Barcelona; 08193, Cerdanyola del Vallès, Catalonia, Spain

^b Institute of Neurosciences, Universitat Autònoma de Barcelona, 08193, Cerdanyola del Vallès, Catalonia, Spain

ARTICLE INFO

Keywords:

Biomembranes
Ion channels
TRP channels
Lipid-protein interactions
Paralipidome
Martini force field
Bioactive lipids

ABSTRACT

In this study, we characterize the plasma membrane paralipidome of the entire TRPV subfamily using microsecond coarse-grained molecular dynamics (CG-MD) simulations. We describe the lipids in the immediate protein environment, identify lipid binding regions, and map the nature of the binding sites. Key lipid interactions include cholesterol, phosphatidylinositols, phosphatidylserine, and phosphatidylethanolamine. Cholesterol shows preferential and stable binding driven by hydrophobicity to specific and conserved regions in the transmembrane domain. Phosphatidylinositols are located in polybasic patches close to the cytosolic side of the bilayer. Our findings reveal long-lasting specific interactions in previously described binding sites, but also novel lipid pockets, mapped by residue type and conservation. Our approach confirms known and uncovers new bioactive lipid binding sites, and through deeper analysis, we show lipids overlapping with drug-binding sites, which may open opportunities for lipid-based therapies and drug discovery in membrane proteins.

1. Introduction

Integral membrane proteins (IMPs) are embedded in a heterogeneous, asymmetric lipid bilayer forming the cell membrane [1]. As such, the interactions between these elements (lipid-lipid, protein-protein, and lipid-protein) define and modulate the properties of the biomembrane. Lipid-protein interactions (LPis) have long been considered architectural, however specific lipid-proteins interactions important for function are less characterized. High-resolution cryo electron microscopy (Cryo-EM) is paving the way to identify protein-lipid interactions in IMPs [2,3], together with a growing body of experimental evidence showing how lipids modulate membrane proteins changing the collective properties of the membrane [4].

Structural data regarding protein-lipid interactions is still limited. Only structures with high enough resolution allow to assign non-protein densities to lipids, and even those with high resolution often face problems to determine the exact headgroup of the lipid. IMPs heterologous expression and purification process inherently affects the lipid microenvironment, biasing lipids bound to the protein. Besides, dynamic properties of IMPs and protein-lipid interactions are not captured,

only those with high and stable affinities. Molecular dynamics arise as an excellent partner tool to structural data, allowing to simulate IMPs with a customized lipid bilayer that more closely resembles their native conditions, and study the dynamic behavior of specific protein-lipid interactions [5–7].

An important set of IMPs are Transient Receptor Potential (TRP) ion channels, the second largest ion channel superfamily [8,9]. The TRP vanilloid subfamily (TRPV) consists of six members which are widely expressed in many tissues including different parts of the nervous system, heart, kidneys, skin, and intestine, among others [10–12], being TRPV1 the most representative channel of the subfamily, the noxious heat sensor [13,14]. The physiological roles of this subfamily are vast, such as nociception, cardiovascular functions, immunity, temperature sensing, mechanotransduction, or intestinal and kidney calcium reabsorption [15–17]. TRPV1–4, also named “thermoTRPVs”, are non-selective, heat-sensitive cation channels, whereas TRPV5–6 are highly selective for Ca^{2+} and have not been shown to respond to temperature changes [18,19]. All six members of the TRPV family are structurally well characterized homotetramers and share a common topology consisting of six transmembrane regions (S1–S6), a voltage-sensor-like

* Corresponding author at: Unit of Biophysics, Department of Biochemistry and Molecular Biology, Facultat de Medicina, Av. Can Domènec s/n, Universitat Autònoma de Barcelona; 08193, Cerdanyola del Vallès, Catalonia, Spain.

E-mail address: alex.peralvarez@uab.cat (A. Peralvarez-Marín).

¹ These authors contributed equally.

domain (VSLD) between S1-S4, a pore-forming loop between S5 and S6, and large intracellular C-terminal, containing the TRP box, and N-terminal, containing an ankyrin repeat domain (ARD), domains important for tetrameric assembly, connected to the S1 by the membrane proximal domain (MPD or pre-S1) [20–23].

Biochemical and structural studies have shown that phospholipids and sterols interact and modulate TRPVs activity [24,25]. Competitive ligand-lipid binding at the interfacial phase and the hydrophobic core depending on subcellular localization may account for on-off states for TRPVs [26,27]. Lipids do not only play a functional and structural role in ligand-free TRPVs, but they can also directly affect the activity of other ligands, highlighting the crucial importance of characterizing the lipidic microenvironment of TRPVs to better understand their biology and pharmacology.

Therefore, the objectives of this study are to characterize the paralipidome of TRPV channels using long-timescale CG-MD simulations, focusing on how specific lipid species populate the immediate protein environment. Specifically, we aim to identify lipid-binding regions on the channels and assign the protein residues mediating lipid recognition, with particular attention to their conservation and chemical nature.

Hence, we have performed 15 μ s CG-MD simulations of TRPV channels and systematically mapped the plasma membrane paralipidome [28]. Our analysis revealed both transient and long-lasting

lipid interactions, including specific contacts in previously described binding sites as well as novel lipid-binding pockets. We further assigned the relevant TRPVs residues for lipid-dependent binding and compared TRPVs lipid-binding sites with known drug-binding sites, leading to the discussion of possible pharmacological implications and potential drug design and discovery opportunities.

2. Results & discussion

2.1. Simulation set-up

To study the LPIS between the TRPV channels and a representative plasma membrane, we have put the six TRP channels of the vanilloid subfamily (TRPV1, TRPV2, TRPV3, TRPV4, TRPV5, and TRPV6) in a 10-lipid plasma membrane (Fig. 1) and simulated them using CG-MD for 5 μ s in 3 independent replicas, with a total simulation time of 15 μ s for each channel and 75 μ s in total for the study. To do so, we have used the composition defined by Ingólfsson et al. [29] with minor modifications (Table 1). Overall, both leaflets contained cholesterol (CHOL), 1-palmitoyl-2-oleoyl phosphatidylcholine (POPC), 1-stearoyl-2-arachidonoyl phosphatidylcholine (PAPC), 1-palmitoyl-2-oleoyl phosphatidylethanolamine (POPE), dilinoleoyl phosphatidylethanolamine (DIPE), and N-stearoyl-D-*erythro* sphingomyelin (DPSM); while the lower leaflet

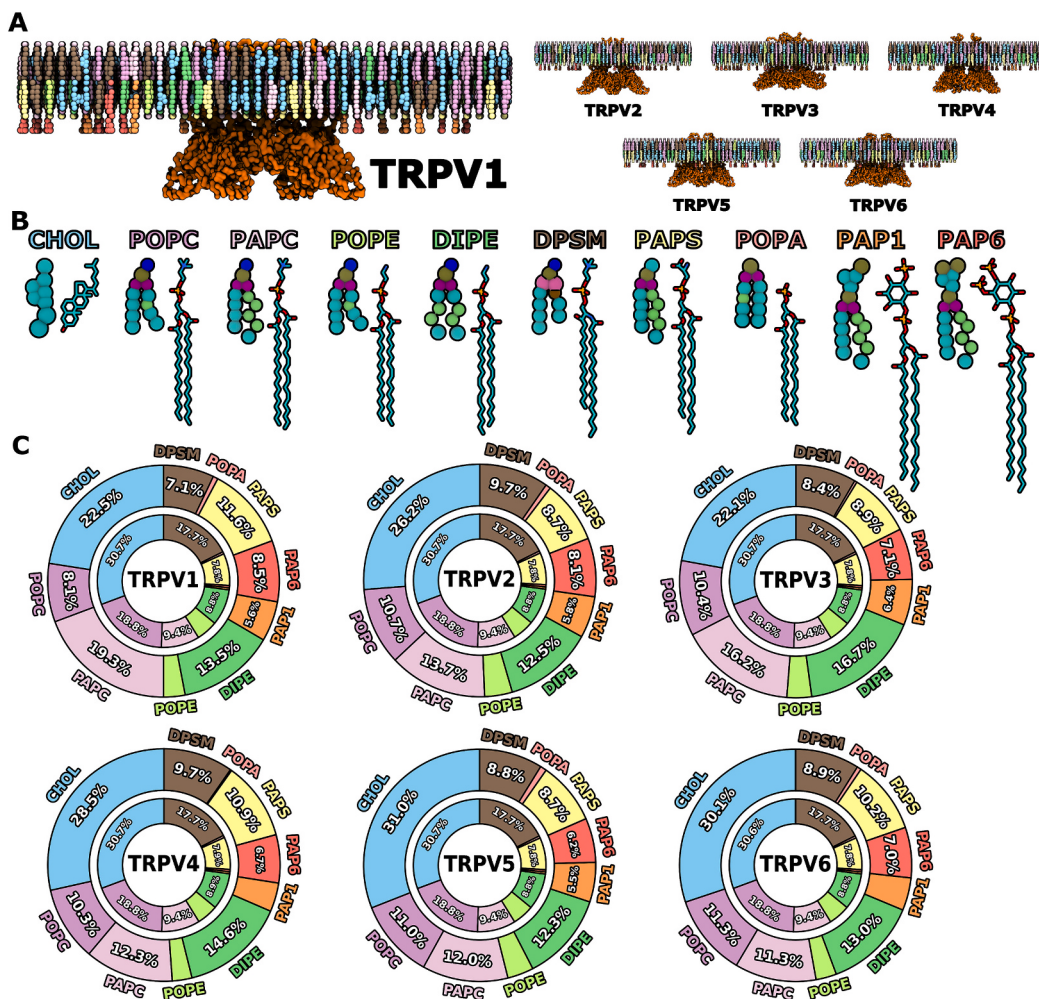


Fig. 1. System set-ups and lipid depletion-enrichment. (A) Side view of the initial system set-up for the coarse-grained molecular dynamics simulations. Lipids are shown as Van der Waals representations, colored by lipid type. Proteins are represented as a surface representation of the backbone beads. Water and ions are omitted for clarity. (B) List of lipids used for the simulations. For each lipid, the coarse-grained Martini 2.2 (left) and the corresponding atomistic (right) representations are showed. (C) Lipid depletion-enrichment around each TRPV subtype. The inner donut indicates the initial membrane composition. The outer donut shows the average lipid composition around the protein (< 0.5 nm) during the last 500 ns of the simulations.

Table 1
Membrane composition.

Leaflet	CHOL	POPC	PAPC	POPE	DIPE	DPSM	PAPS	POPA	PAP1	PAP6
Upper	32.0 %	24.0 %	12.0 %	6.0 %	2.0 %	24.0 %				
Lower	29.1 %	13.5 %	6.7 %	4.5 %	15.7 %	11.2 %	15.7 %	1.1 %	1.1 %	1.1 %

additionally contained 1-stearoyl-2-arachidonoyl phosphatidylserine (PAPS), 1-palmitoyl-2-oleoyl phosphatidic acid (POPA), 1-stearoyl-2-arachidonoyl phosphatidylinositol-3-phosphate (PAP1), and 1-stearoyl-2-arachidonoyl phosphatidylinositol-4,5-biphosphate (PAP6). Phosphatidic acid (PA) was chosen because POPA and lysophosphatidyl phosphatidic acid (LPA) have been shown to interact with TRPVs, particularly with the membrane proximal domain (MPD) of TRPV1 and TRPV2, in TRPV1 C-terminus [30–33], and between S3 and S4-S5 linker in TRPV2 [34]. Phosphatidylinositol-3-phosphate (PAP1) was added to the composition as a potential competitive counterpart of the phosphatidylinositol-4,5-biphosphate (PAP6), which is a well-known TRPV modulator, [35–37] to determine whether TRPVs have a specific affinity towards biphosphate inositols.

2.2. Depletion-enrichment of lipids around each TRPV

Comparing the initial membrane composition to the final lipid shell surrounding each protein at the end of the simulations allows for determination of the depletion or enrichment of each lipid around the TRPV channels. Due to LPiS, the lipids closest to the protein show reduced dynamics and are slower to exchange –usually referred as lipid annulus-, demonstrating distinct capacities from those in the bulk membrane [38].

Regardless the TRPV, phosphatidylinositol species (PAP1 and PAP6) were enriched by 12 and 14-fold, respectively (Fig. 1C and Table S1), a phenomenon previously described for many other membrane proteins, including ion channels, in both computational and biochemical studies [6,39–41]. Polyunsaturated (PU) lipids, such PAPC, DIPE, and PAPS were also enriched (Table S2), which is coupled to a depletion of the monounsaturated (MU) lipids, such as POPC, POPE, and DPSM. POPC and POPE share the headgroup with PAPC and DIPE, respectively, which indicates that TRPVs favor interactions with lipids that possess more flexible acyl chains, pointing to higher facility of these lipids to explore the different cavities and binding regions in membrane proteins. POPA on the other hand, was mostly depleted around the six TRPV channels. This includes TRPV1 and TRPV2, for which experimental data shows that DPPA binds the N-terminus MPD domain [30], and LPA binds to the C-terminus of TRPV1 [33]. Biochemical *in vitro* data was obtained by doping lipids with purified MDP domains with pure lipid samples at high non-physiological concentrations (> 50 μM). Even in functional assays, TRPV2 is activated in the presence of PA [42]. POPA is present at much lower concentration in our computational setup, probably competing in terms of affinity with PAP1 and PAP6, arguing for either a more prevalent role for phosphatidylinositol (PI) for TRPVs function, and/or the more flexible PU tail of PAP1 and PAP6 allowing deeper cavity scouting. Thus, lipid binding and its potential protein regulatory role is influenced by the presence of other lipids in the bilayer mixture, emphasizing the power of computational studies when biochemical data is available, but also the discovery potential of *in silico* lipidomics-like strategies.

CHOL depletion-enrichment shows a TRPV-dependent pattern. TRPV1–3 depleted CHOL from 30.7 % in the initial composition to 21.6 %, 26.4 %, and 24.2 %, respectively. On the other hand, no remarkable decrease is observed for non-thermoTRPVs, TRPV5 and TRPV6 (29.9 % and 31.2 %, respectively), as well as for TRPV4 (27.9 %). However, due to the high concentration of CHOL in mammalian plasma membranes [29,43] mild depletion or lack of enrichment is compatible with a sufficient number of CHOL molecules around the protein to bind and exert a regulatory role [26,44].

2.3. Lipid residence time and binding events as a proxy for binding affinity

TRPV channels are four-fold symmetry tetrameric structures, so for sampling purposes, each chain becomes a replica, achieving a higher sampling time of ca. ~60 μs of simulation time per TRPV monomer. In fact, of the 317,045 binding events observed in all the simulations (Table S3 and Table S4), 72.8 ± 4.8 % of these events have been observed across at least two chains, implying that, for sampling purposes, each chain can be considered an independent replica. Because of that, the following analyses show the results averaged for all four chains.

Beyond the concept of lipid annulus discussed in the previous section, we have also analyzed the interacting regions of lipids in the TRPV channels structures. We have clustered the residence time of binding events into “known lipid regulators” (Fig. 2) and “non-regulatory” (Fig. 3) lipids, although we are aware of the misconception of such definition, which has biased the understanding of the molecular determinants of LPiS in membrane biology [45]. For TRPVs, emphasis has been put into PI as regulatory lipids, obviating some “non-regulatory” lipids such as PC, PS, PE, PG head groups. In our study, PI lipids show prevalent and relevant binding affinity, represented by the residence time of the lipid sitting at a specific site (Fig. 2, Fig. 3, Fig. S1 and Table S1), arguing for more than a mere membrane architecture role. Beyond the scope of the present study, one key question arising is how LPiS interplay regarding relative amounts of lipid depending on membrane lipid composition, and the determination of lipid binding affinities through structural computational studies.

CHOL, on the other hand, shows preferential binding to helices S4-S6 in all TRPVs (Fig. 2 and Fig. S1), but also to the helices S1 (in TRPV1, TRPV2, TRPV4, TRPV5, and TRPV6), S2 (TRPV1, TRPV4, TRPV5, TRPV6), and S3 (TRPV2, TRPV3, TRPV4, TRPV5, TRPV6). Moreover, CHOL also binds to the S4-S5 linker region to all channels except for TRPV3, and to the TRP box in TRPV3, TRPV5, and TRPV6 (Fig. S1). POPA, even though it suffered an almost complete depletion for all TRPVs, does show binding events in TRPV3 (in S3 helix and S4-S5 linker) and TRPV5 (S1 and S5 helices). Intriguingly, POPA does not show binding for TRPV2 [34] nor for any of the channels that lysophosphatidylcholine A (LPA) and DPPA have been shown to regulate (TRPV1, TRPV2, or TRPV4) [32,33,46,47]. The PI lipids (PAP1 and PAP6) enrichment in TRPVs is significant (Fig. 1, Fig. 2 and Fig. S1) and almost overlapping, especially in the S2-S3 helices and cytosolic loops of the TRPVs TMD, but also in the MPD and C-terminal domains (including the TRP box), where these lipid bindings have been predicted computationally and determined biochemically [48]. Interestingly, POPA shows transient bindings in the same regions (S2-S3 helices, MPD and C-terminal domains) as PAP1 and PAP6, and even in TRPV3 and TRPV5, the stable POPA binding regions are close to the PAP1 and PAP6 bindings (Fig. S1). This fact argues for relevance of the length, occupancy (single/dual tail), and saturation (saturated/unsaturated) of the phospholipid tail, and the possibility that PA may share the same binding regions of PI and/or CHOL but with lower affinity.

Regarding non-regulatory lipids, PC lipids only show significant residence time bind between S1-S2 in TRPV5 and S5 helix in TRPV6 (POPC), and in the S6 helix of TRPV2 (PAPC) (Fig. 3 and Fig. S1). For PE lipids, POPE does not show significant binding to any TRPV channel, whereas DIPE, shows preferential binding to MPD in TRPV1 and TRPV4, to the S2 helix in TRPV4, the S3 helix in TRPV2 and TRPV5, and the S5 helix in TRPV3, TRPV4 and TRPV5 (Fig. 3 and Fig. S1). TRPV4 is the only channel showing significant binding preference for DPSM (in the S4

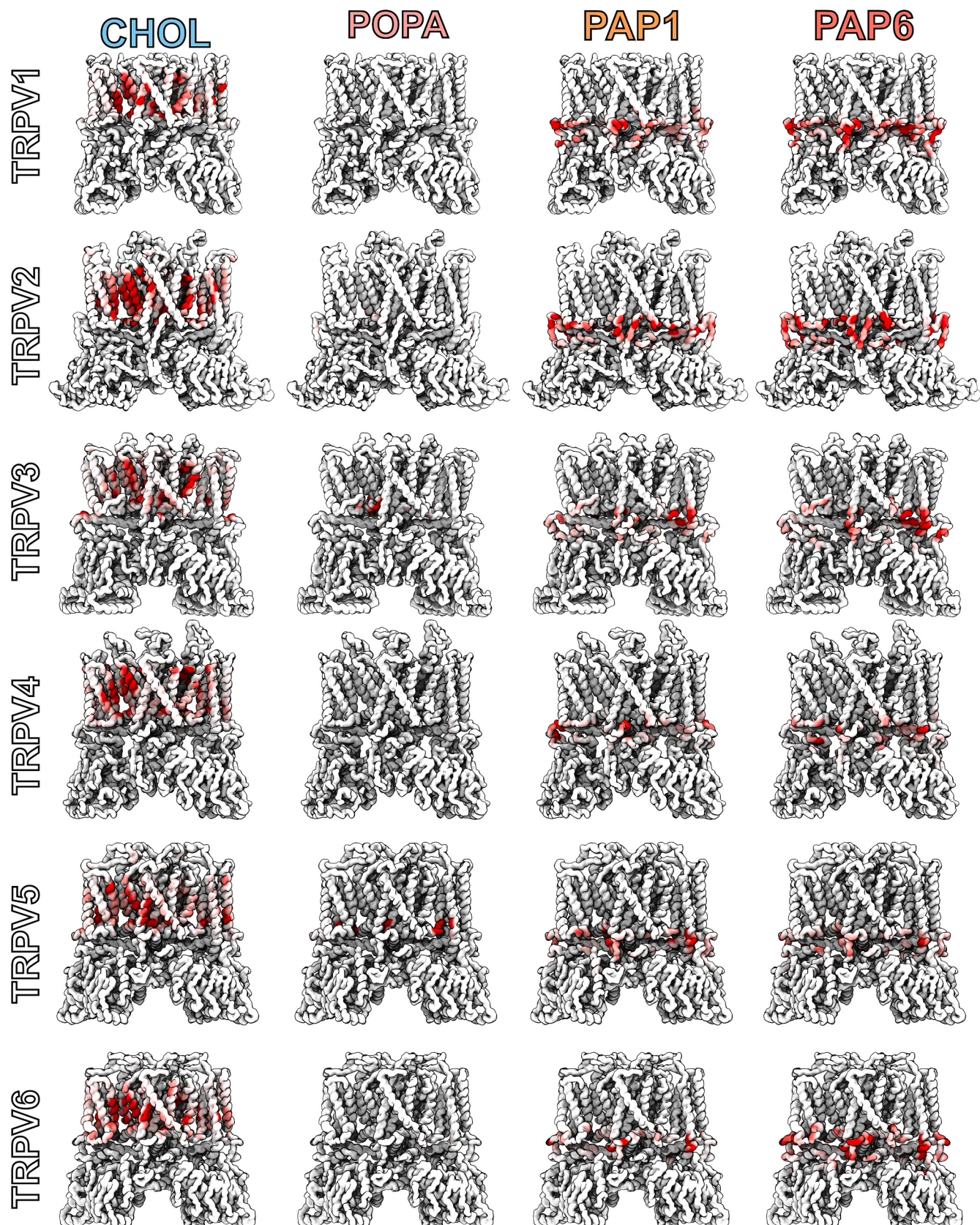


Fig. 2. Known regulatory lipids residence times. The longest residence time per residue is plotted on the surface representation of each TRPV backbone bead. Color spans from 0 μ s (white) to 5 μ s (red).

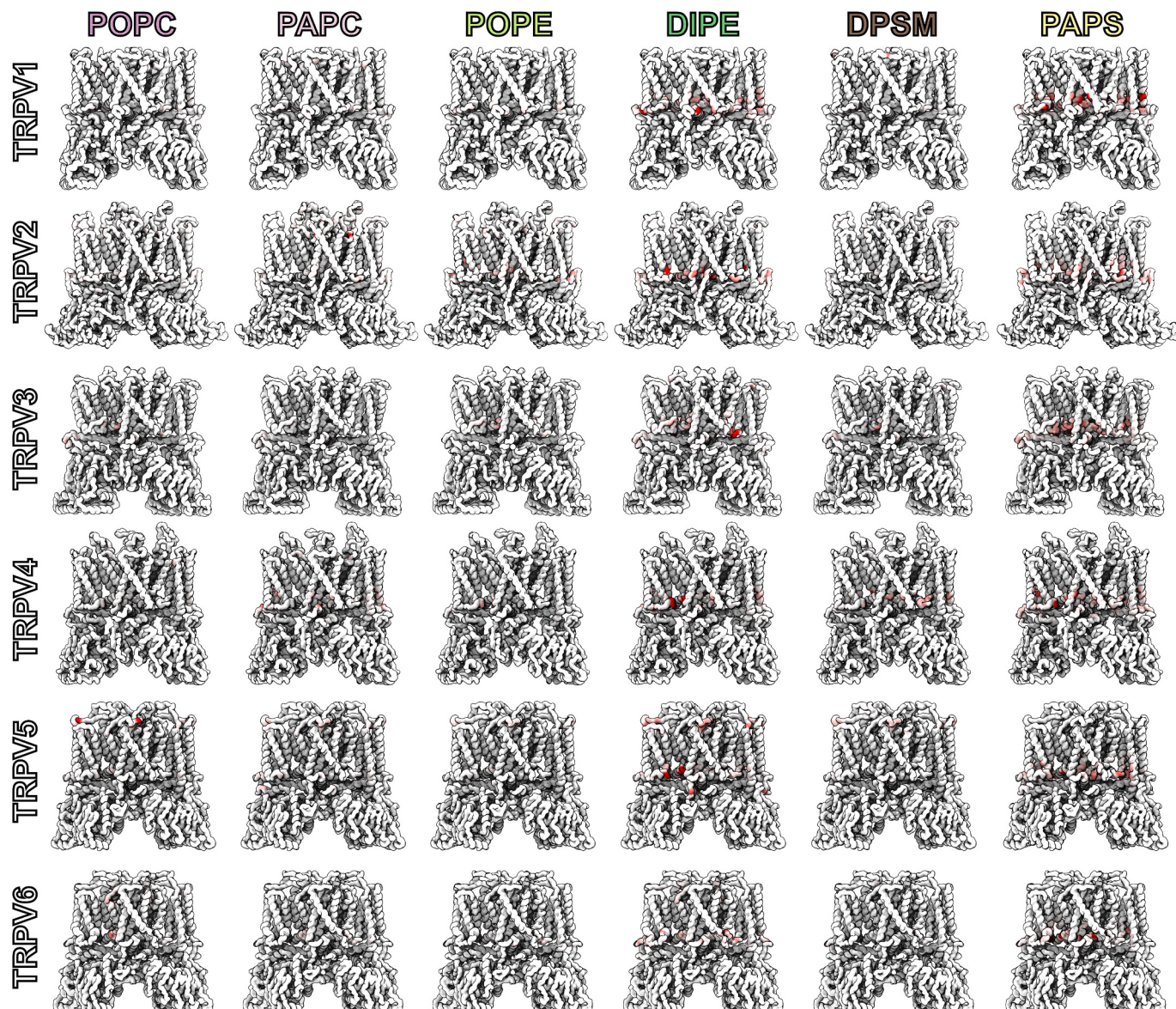


Fig. 3. Non-regulatory lipids residence times. The longest residence time per residue is plotted on the surface representation of each TRPV backbone bead. Color spans from 0 μ s (white) to 5 μ s (red).

helix), which has only been previously linked to TRPV1 [49,50]. Finally, PAPS distributes along all TRPVs (but with higher residence time in the TRPV1, TRPV4, TRPV5, and TRPV6 channels) in the cytosolic side of the TMD, following the positive-inside rule [51,52], as previously observed for TRPV1 [53].

2.4. Characterization of the bioactive paralipidome

Each protein can modulate and select a different lipid environment, that is, a singular lipid composition in the immediate space close to the protein structure which affects to protein function or activation [4]. Levental & Lyman coined the term *paralipidome* to refer to this local lipid environment. Depending on the protein state or conformation, each protein can change or modify its local lipid environment. In our simulations, we observe how each protein of the TRPV subfamily relates to its apo state paralipidome, which we have characterized owing to CG-MD simulations. Further characterization with CG-MD may lead to extensive sampling in different gating states by extending the simulation time over 100 μ s to explore competitive binding and binding affinity [5,6]. Here we define that the bioactive paralipidome of the six TRPV channels

includes sterols (CHOL), and phosphatidylinositols (PAP1 and PAP6) (Fig. 2, Fig. S1). Besides, the bioactive paralipidome of channels TRPV1–5 contains phosphatidylethanolamine (DIPE) as well (Fig. 3, Fig. S1). The bioactive paralipidome of TRPV1 and TRPV4–6 also comprises phosphatidylserine (PAPS) (Fig. 3, Fig. S1), for TRPV3 and TRPV5 incorporates phosphatidic acid (POPA) (Fig. 2, Fig. S1), and TRPV4 bioactive paralipidome is the only one to involve sphingomyelin (DPSM) and phosphatidylcholine (PAPC) (Fig. 3, Fig. S1).

The relationship between TRPV channels and CHOL has been reported several times in the literature, [26,54–59] and similarly for the relevance of PAP1 and PAP6 in the TRPVs lipid fingerprinting. [35–37,48] Nonetheless, we have also found some interactions which have not been previously described. First, even though relation between TRPV1 and ethanolamines was previously reported [60], here we find the binding of phosphatidylethanolamine to –several– TRPV channels. Phosphatidylserine (PAPS) has been related to TRPV1, [53] but here we have also seen important binding of phosphatidylserine to TRPV4–6. Phosphatidic acid in both the phospholipid and lysophospholipid fashion has been linked to TRPV1 and TRPV2, [30–34] but here PA is only linked to TRPV3 and TRPV5. Sphingomyelin has been previously

related to TRPV1, [49,50] but in our simulations DPSM binds to TRPV4, opening new leads on the role of sphingomyelin in TRPVs physiology.

2.5. Molecular determinants of lipid binding

2.5.1. Residue nature

Lipids interact with certain regions in TRPVs driven by physico-chemical affinities. These LPs need to be stable and involve at least four residues to be considered as *binding sites* (more details are provided in

the Methods section). From here on, we start talking about binding sites, instead of interacting regions as discussed hitherto. In fact, as reported for the first time in 1999, lipids can also bind to ligand pockets and enter the transmembrane protein structure, becoming specific lipid binding sites with apparent binding affinities [4,61,62].

To better understand the nature of TRPV-lipid interaction, we have defined and implemented a weighted GRAVY score (details in the Methods section) to further characterize the TRPVs lipid binding sites in terms of residue hydrophobicity, recurrence (number of events) and

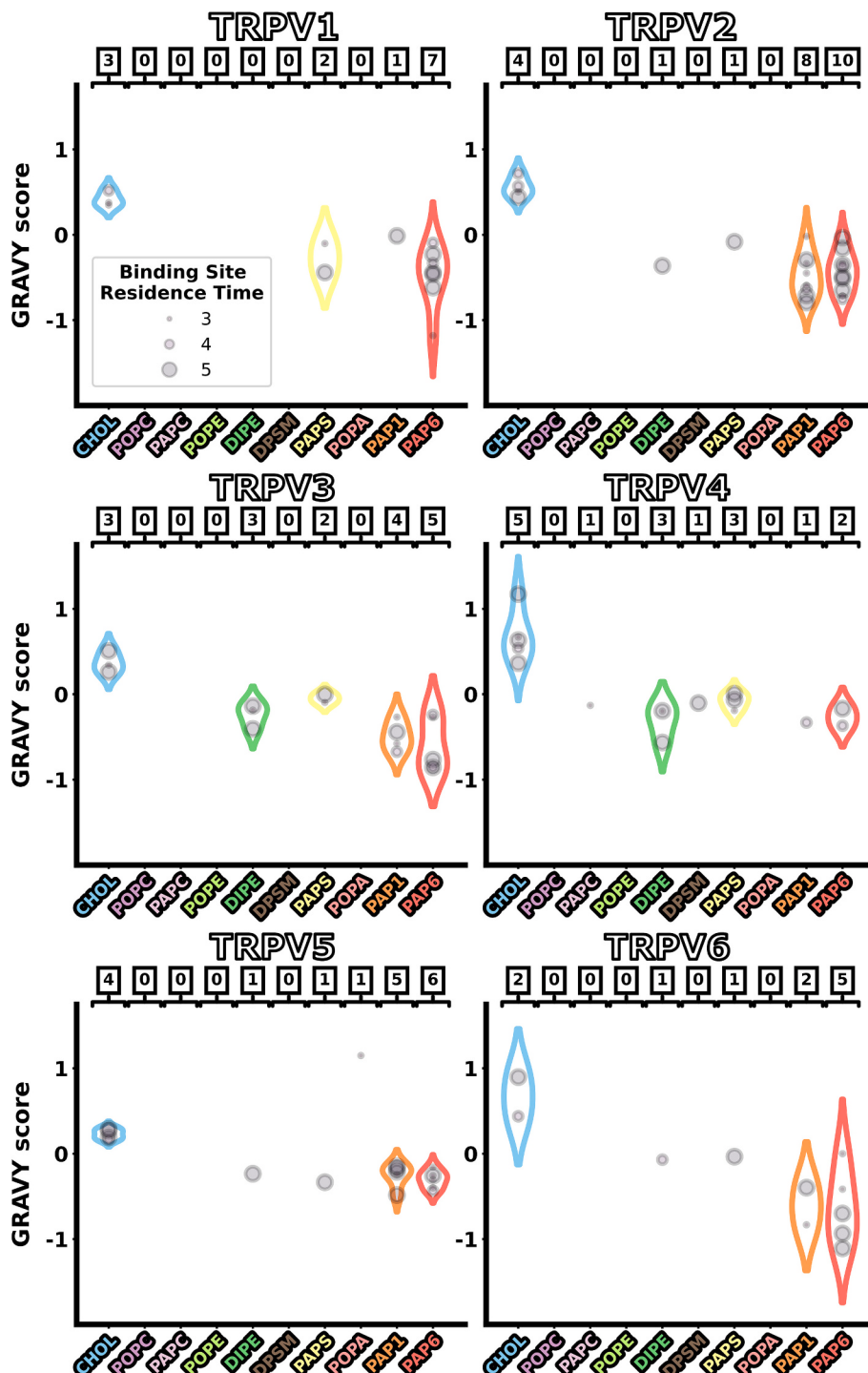


Fig. 4. GRAVY score of lipid binding sites. Each TRPV subplot shows the number of binding events per lipid type. The events are size coded according to their residence time, as calculated by PyLipid. The y axis shows the weighted average GRAVY score. The number of binding events is indicated above each lipid type. The violin plot is used to represent the points distribution and standard deviation for each lipid.

residence time (Fig. 4). Taken together the results from the previous section and Fig. 4, the most relevant LPis are PI lipids (35 and 21 binding sites across all six TRPV channels for PAP6 and PAP1, respectively), CHOL (21 binding sites), PAPS (10 binding sites), and DIPE (9 binding sites), whereas the lipids with the least binding events are POPA, PAPC and DPSM (1 each), and POPC and POPE (0).

Fig. S2 (known regulatory lipids) and Fig. S3 (non-regulatory lipids) show the frequency of each type of amino acid to participate in each lipid binding. Regarding the type and nature of the residues binding each lipid, CHOL binds to hydrophobic residues (Fig. 4), GRAVY score values close to 1), mostly to hydrophobic Leu, Ile, Val and aromatic Phe and Tyr (Fig. S2). PAP1 and PAP6 bind to positively charged residues (Fig. 4, negative GRAVY score values), Arg and Lys, but also to aromatic Phe and Trp (Fig. S2). Last, PAPS and DIPE show higher residue variability (Fig. 4), with binding across all kinds of residues (Fig. S3), suggesting that the binding might not be as specific as in previous cases.

Dissection of the residues participating in LPis in TRPV channels allows for definition of specific lipid-binding sites. Taken altogether, our data indicates that TRPV-lipid interactions are physicochemically specific, arguing for a TRPV paralipidome in terms of function interplay between LPis and endogenous/exogenous agonist/antagonist-driven channel gating.

2.5.2. Characterization of lipid binding sites

Fig. 5 shows the TRPV lipid binding sites differentiated by lipid and TRPV subunit. The minimum residence time to consider a binding site is of 2.5 μs, i.e. 50 % of the simulation average time, as a probe to define the whole lipid binding sites taking into account the following: i) simulations allow to identify strong and transient LPis depending on residence time, and ii) residue conservation will act as beacon for conserved lipid binding sites across the TRPV subfamily, whereas divergence will account for specific TRPV channels lipid binding sites (Fig. S4 for complete multiple sequence alignment). We have grouped the lipid bindings into four previously described TRPV binding sites: vanilloid, shallow S4-S5, S2-S3 site, and S1-S4 base [63]. Further, we have found and defined two novel lipid binding sites, which we have tentatively named upper vanilloid and shallow S2-S3 sites. The molecular representation of these six binding sites is shown in Fig. S5. The vanilloid site is primarily located at the short S4-S5 helix, which connects helices S4 and S5. However, lipid stabilization in this pocket also involves contributions from residues in the S1-S4 and S5-S6 helices (Table 2). The upper vanilloid binding site represents a distinct lipid-binding region positioned above the vanilloid site, where lipids are mainly stabilized by interactions with residues in the S5-S6 helices. The shallow S4-S5 binding site is located posterior to the vanilloid pocket and is largely formed by residues from the N-terminal MPD (NMPD) and the S1-S4 helices. The S2-S3 site is centered around the short S2-S3 helix that

connects helices S2 and S3, but stabilization often extends to involve residues from the S4-S5 helix and, in some cases, the S5-S6 helices. In close proximity, the newly defined shallow S2-S3 site refers to a more superficial region relative to the canonical S2-S3 site. This site lies closer to the TRP domain and is primarily stabilized by residues from the S1-S4 helices and the NMPD. Last, the S1-S4 base is located at the lower part of the S1-S4 helices, near the TRP helix. Lipids bound in S1-S4 base are predominantly stabilized by residues from the S1-S4 helices and the C-terminal MPD (CMPD).

2.5.2.1. Phosphatidylinositol. Regarding the lipid types, PI lipids (PAP6 and PAP1) showed the highest number of binding events (35 and 21, respectively, Fig. 4), distributed through several binding sites. All TRPV channels bind PAP6 and PAP1 in the S1-S4 base, except for PAP1 in TRPV3. Besides, TRPV3, TRPV5, and TRPV6 bind PAP1, and PAP6 in the shallow S4-S5 site, whereas TRPV4 binds only PAP6. In TRPV2 PAP1 and PAP6 only bind to the vanilloid site, where PAP6 has been experimentally determined for TRPV1. [64–67] Moreover, PAP1 and PAP6 bind to the S2-S3 site in TRPV2 and TRPV5, and PAP6 in TRPV1 and TRPV6 as well, where a PAP6 has previously been observed for TRPV5, [68] indicating the correlation of our results with already published data. Furthermore, PAP6 is the only lipid that has been able to get stabilized in the new shallow S2-S3 site, in TRPV1 and TRPV2.

2.5.2.2. Cholesterol. CHOL binds primarily to vanilloid site in all six TRPV channels. A cholesterol molecule in the vanilloid pocket has been previously reported for TRPV2 [26]. In addition, CHOL was found to bind to the newly described upper vanilloid binding site in TRPV3 and TRPV4 channels, and the S1-S4 base site in TRPV5.

2.5.2.3. Phosphatidic acid. POPA, the last bioactive lipid, binds to shallow S4-S5 site in TRPV5, close to the region determined experimentally for TRPV1 and TRPV2 [32–34], where 5',6'-epoxyeicosatetraenoic acid (EET) binds in TRPV4 [69].

2.5.2.4. Other lipids. Regarding the structural lipids, PAPS, the one with the highest number of binding sites, is distributed through all TRPVs, binding to the S1-S4 base in TRPV1, TRPV4 and TRPV5, to the vanilloid in TRPV2, and to the S2-S3 site in TRPV1, TRPV3 and TRPV6. DIPE shows binding to TRPV2, TRPV3, TRPV4 and TRPV6 in the vanilloid site, to TRPV3 in the upper vanilloid, and to the S1-S4 base in TRPV4. DPSM and PAPC only show binding to the S1-S4 base in TRPV4. Last, POPE and POPC do not show any binding sites in TRPV channels.

Altogether, these results show that PI lipids and/or CHOL show binding to the six identified binding sites across all six channels, indicating that these lipids to TRPV channels, defining long-lasting interactions for CHOL and PI lipids [4]. PAPS and DIPE show binding to all

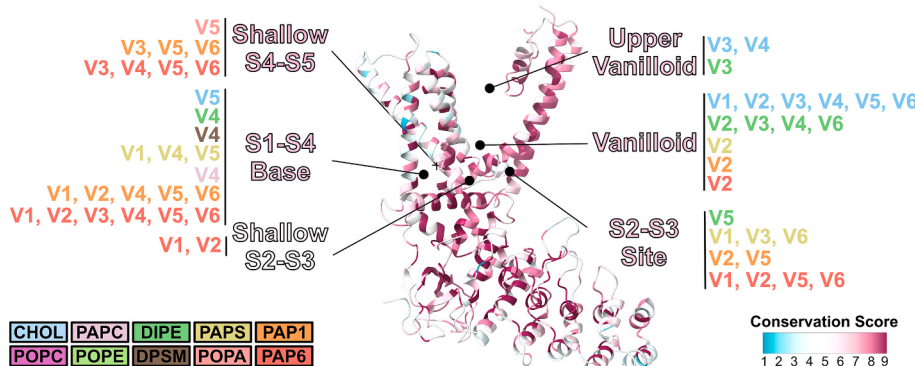


Fig. 5. Summary of binding sites in TRPV channels. A single TRPV subunit is represented as a cartoon, colored by ConSurf [70–75] conservation score. The color of the binding site name represents the computed binding site average, calculated among the residues participating in lipid binding. Molecular representation of lipids binding site can be found in Fig. S4.

Table 2

Binding sites in TRPV channels. Summary of the six lipid binding sites observed in the CG-MD simulations and the ligand described in the Cryo-EM structures in these binding sites. For each binding site, the binding region, the channel, the lipid bound, the domains and residues involved, the conservation score, and the ligands bound to the same binding site are shown.

Binding site	TRPV channel	Lipid	Domains ^a	Residue ID	Conservation score	Ligand
Canonical vanilloid site	1	CHOL	S1-S4 S4-S5 linker S5-S6	Tyr511, Leu515, Phe543, Leu547, Thr550, Asn551, Leu553 Ala566, Ile569, Glu570, Ile573, Leu574	7.7	Capsaicin, RTX, ZEI
	2	CHOL, DIPE, PAP1, PAP6, PAPS	S1-S4 S4-S5 linker S5-S6	Leu577, Cys578, Met581, Val583, Phe587, Phe591, Leu663, Ala666, Leu670 Met468, Tyr471, Phe472, Leu475, Val506, Leu507, Leu510, Asn511 Ser526, Ile529, Gln530, Val532, Ile533, Leu534, Arg535	7.7	2-APB
	3	CHOL, DIPE	S1-S4 S4-S5 linker S5-S6	Phe547, Phe551, Ala628, Leu632, Val635, Leu636 Ser511, Asp512, Ser515, Phe569 Gln570, Ser571, Met572, Leu584, His585	7	THCV, Trpvicin
	4	CHOL, DIPE	S1-S4 S4-S5 linker S5-S6	Leu588, Lys589, Phe592 Asn541, Ser542, Phe544, Ser548, Phe549, Leu552, Ile555, Leu559, Phe580, Ala581, Val583, Leu584, Met587, Asn588 Ser603, Ile606, Gln607, Leu610, Phe611	7.4	
	5	CHOL	S1-S4 S4-S5 linker S5-S6	Arg616, Val620, Phe624, Tyr628, Leu698, Thr701, Leu705, Leu710 Pro424, Phe425, Ile428, Thr431, Leu435, Leu438, Met442, Met447, Gly449, Glu450, Val452, Pro453, Phe456, Val459, Leu460, Cys463, Met466 Phe478, Thr479, Ile482, Gln483, Met485, Ile486, Phe487	7	Oleoyl-CoA, Econazole
	6	CHOL, DIPE	S1-S4 S4-S5 linker S5-S6	Phe416, Gln418, Thr419, Ile420, Phe425, Leu428, Val452, Ser455, Phe456, Val459, Leu460, Cys463, Met466, Phe478, Ile482, Gln483, Met485, Ile486, Phe487, Leu490, Met491, Cys494, Ala498, Val500, Ile501, Phe504, Pro527, Leu530, Phe531, Phe534, Phe553, Met554, Ile557, Thr558, Ala560, Ala561, Ile564, Ile565, Leu569, Met570 Met528	5.8	THCV, 5GK, 81F, Genistein, PCHPD1, PCHPD2, PCHPD3, PCHPD4, PCHPD5
Upper vanilloid site	3	CHOL, DIPE	S1-S4 S4-S5 linker S5-S6	Leu530, Phe531, Phe534, Phe553, Met554, Ser556, Ile557, Thr558, Ala560, Ala561, Ile564, Ile565, Leu569, Met570, Leu573 Ala549 Leu584, His585	7.1	
	4	CHOL	S5-S6	Leu614, Leu618, Tyr621, Met625, Glu664, Ser667, Thr668, Leu670, Leu671, Phe674, Met685, Pro692, Val693, Ile696, Ile697, Val700, Ile704	6.9	
Shallow S4-S5	3	PAP1, PAP6	S1-S4 NMPD S1-S4 S4-S5 linker CMPD	Phe416, Gly417, Phe487, Gly488, Arg492 His430, Trp433, Lys434 Lys438, His439, Phe441, Phe442, Phe445, Gly568, Phe569 Gln570 Trp692, Arg693, Arg696	7	
	4	PAP6	NMPD S1-S4 S4-S5 linker CMPD	Asn456, Arg460, Trp463 Leu596 Lys597 Lys727, Lys730, His731, Trp733, Lys734, Trp737	7.8	
	5	PAP1, PAP6, POPA	NMPD S1-S4 S4-S5 linker CMPD	Lys314, Ser318, Trp321, Lys322 Arg326, Gly471, Phe472 Gln473 Trp593, Arg594	7.4	
	6	PAP1, PAP6	NMPD S1-S4 S5-S6 Trp593	Ser318, Trp321, Lys322, Arg326 Phe472, Gln473 Trp593	7.1	Econazole
	1	PAP6, PAPS	S1-S4 S4-S5 linker S5-S6 CMPD	Phe507, Val508, Phe559 Gln560, Gln561, Lys571, Leu574, Arg575 Arg579, Lys695 Trp698	7.8	

(continued on next page)

Table 2 (continued)

Binding site	TRPV channel	Lipid	Domains ^a	Residue ID	Conservation score	Ligand
	2	PAP1, PAP6	NMPD S1-S4 S4-S5 linker	Lys365, Pro367, Arg369 Trp464, Ile465, Ser466, Phe467, Met468 Lys531, Arg535	6.9	
	3	PAPS	S1S4 S4-S5 linker	Ser515, Ile516 Gln570, Ser571, Leu584, His585	7.5	
	5	DIPE, PAP1, PAP6	S5S6 NMPD S1-S4 S4-S5	Lys589, Phe592 Lys300, Arg302 Arg414, Gly417, Gln418, Thr419, Pro424 Gln483, Lys484, Phe487	7.1	
Shallow S2-S3	6	PAP6, PAPS	S1S4	Phe416, Gly417, Phe487, Gly488, Arg492	4.2	
	1	PAP6	NMPD	Lys332 ^b , Gly334 ^b , Met335 ^b , Lys393, Asn394, Tyr402, Ser403, Ser404	6.7	
	2	PAP6	S1-S4	Gln498, Arg499, Arg500, Pro501		
			NMPD	Lys201 ^b , His202 ^b , Gln294 ^b , Lys304 ^b , Trp351, Lys353, Asn354, His363	5.8	
Base S1-S4	1	PAP1, PAP6, PAPS	S1-S4 CMPD	Trp454, Trp457, Arg458, Arg459, Arg460, Leu461, Ile465 Asn673, Trp676, Trp677, Arg679	6.8	
	2	PAP1, PAP6	NMPD	Asp425, Arg429 Phe430, Arg433 CMPD	5.9	
	3	PAP6	S1-S4	Phe721, Arg722, Ser723, Gly724, Lys725, Arg744		
			CMPD	Trp351, Lys353 Trp454, Arg458		
	4	DIPE, DPSM, PAP1, PAP6, PAPC, PAPS	S1S4	Asn474, Phe524, Thr527, Asn528, Asp531, Asp546, Gln550, Tyr553, Tyr591, Phe592	7.6	9QM, X7N, XQ3, XPW, XS9
	5	CHOL, PAP1, PAP6, PAPS	CMPD S1-S4 S5-S6	Thr739, Thr740, Asp743, Ser747, Phe748 Gln27 ^c , Phe319, Lys320, Lys323 Tyr324, Pro327, Glu403, Tyr415, Leu421, Gly422, Tyr467 Thr600, Met603, Lys607, Pro609, Arg610, Phe611, Leu612, Trp613, Pro614, Arg615, Ser616	6.7	O6S
	6	PAP1, PAP6	CMPD NMPD	Trp629 Cys157 ^b , Leu319, Lys322, Arg323, Tyr324, Arg326, Pro327	8.6	
			CMPD	Arg632		

^a Domain definition corresponds to the following residues in each TRPV channel: **NMPD**: 366-429 for TRPV1; 326-388 for TRPV2; 373-435 for TRPV3; 402-465 for TRPV4; 263-323 for TRPV5; 302-362 for TRPV6. **S1S4**: 430-559 for TRPV1; 389-519 for TRPV2; 436-569 for TRPV3; 466-596 for TRPV4; 324-472 for TRPV5; 363-511 for TRPV6. **S4S5**: 560-576 for TRPV1; 520-536 for TRPV2; 570-586 for TRPV3; 597-613 for TRPV4; 473-489 for TRPV5; 512-528 for TRPV6. **S5S6**: 577-691 for TRPV1; 537-653 for TRPV2; 587-685 for TRPV3; 614-726 for TRPV4; 490-586 for TRPV5; 529-625 for TRPV6. **CMPD**: 692-end for TRPV1; 654-end for TRPV2; 686-end for TRPV3; 727-end for TRPV4; 587-end for TRPV5; 626-end for TRPV6.

^b Residues actually located in the ARD

^c Residues actually located in the distal N-terminus

TRPV channels (except for DIPE in TRPV1), but are not distributed through the six binding sites, indicating more limited stabilization. Last, POPA, DPSM and PAPC are only bound in one binding site and channel.

2.5.3. Residue conservation

Lipid-protein interactions are specific. Discrete lipid binding regions have been characterized experimentally and predicted through bioinformatics. In our study, regardless of the force field limitations, we can assign preferential lipid binding and dynamics for specific residues in TRPV channels CHOL-protein interaction regions within the TMD (i.e. S1S4 and S5S6 domains). The NMPD, CMPD, and S4S5 domains are hubs for PIs, but also for other lipids, such as PE, PS, and PA, which should be regarded putatively, at least from the apparent affinity derived from residence time, as bioactive lipids. TRPV1 to TRPV6 show high degree of conservation in the common structural scaffold, ranging from the resolved N-terminal to the C-terminal membrane proximal domains, and single residue variations allow to define specific lipid-protein interactions, especially in the NMPD when comparing the TRPV1–4 to the TRPV5–6 subgroups (Table 2 and Fig. 5). This high degree of conservation is also evident across the six previously described binding sites. Vanilloid binding site exhibits a conservation score of 7.1 across all six channels, while the upper vanilloid conservation score is 7. The shallow S4-S5 conservation score is 7.3, the S2-S3 site conservation score is 6.7,

the shallow S2-S3 conservation score is 6.25, and S1-S4 base conservation score of 6.9.

Another key aspect is how the non-resolved distal N- and C-terminal domains, which are highly divergent among TRPVs, are implicated in these LPi. TRPV1, TRPV2, and TRPV6 show that the ARD binds the longer stearoyl and arachidonoyl acyl chains of PAP1 and PAP6. The elastic network prevents the protein to undergo conformational changes, but it is easy to speculate that long distance ARD-Pi interactions may play a crucial role in the gating mechanism. The distal and divergent N-terminus of TRPV5 which structure is resolved, participates in the binding of several lipid through Gln27 (Table 2), arguing for the role of the disordered and divergent N-terminus of TRPV1-TRPV4 in LPi and in the channel function. [37,76]

2.5.4. Comparison of lipid and drug binding to TRPVs

To assess the pharmacological relevance of the lipid binding sites in TRPV channels, we compare previously described drug/lipids binding pockets to the six lipid binding sites identified here across all six TRPV channels (Fig. 6). The detailed mapping of lipid binding sites and overlapping drugs is summarized in Table 2. Remarkably, three of these lipid binding sites are shared with previously described ligand-binding pockets, suggesting a potential behavior of the lipids in stabilizing these ligands or even directly competing for binding. As mentioned

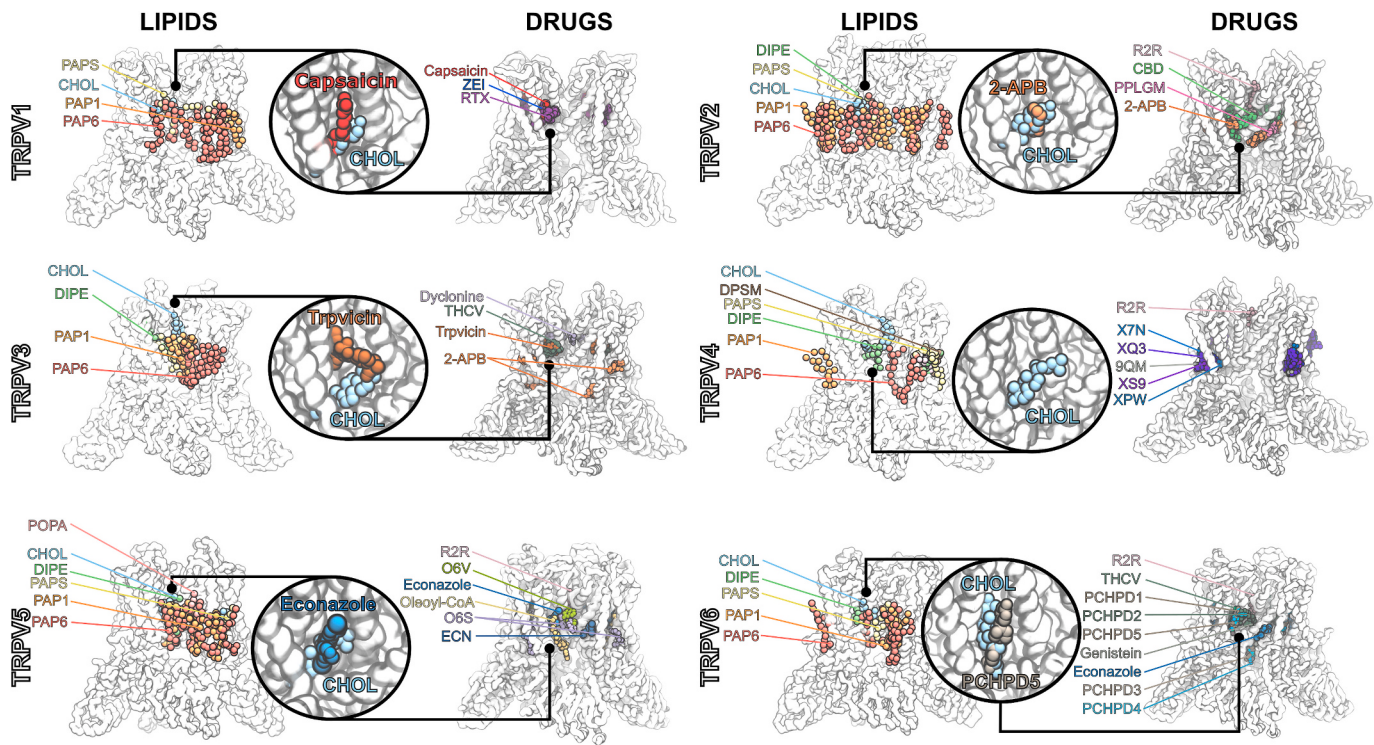


Fig. 6. Representative lipid poses and drugs structurally resolved. For each TRPV, the representative lipid binding pose for each binding event and the structurally resolved drugs available in PDB structures are shown for comparison. Full information of the ligands is described in Table S5. The binding site, lipid, and drug shown in more detail are described in Table S6, detailing the interaction of both lipid and drug binding.

above, TRPV channels possess an intricate regulation wherein exogenous ligands interplay with the endogenous lipids, which could play an essential role modulating their binding via cooperation or competitive binding [37,77–79]. Beyond TRPV1, TRPV channels have limited specific pharmacology, making the discovery of new druggable pockets especially valuable. The overlap between lipid and ligand-binding sites suggests that endogenous lipids may modulate ligand interactions through stabilization or competition, offering promising targets for drug design.

2.5.4.1. Known lipid-drug binding sites. The vanilloid binding site, predominantly occupied mainly by CHOL in our simulations, is a well-established ligand-binding pocket in TRPV channels. Various ligands, such as capsaicin, 2-aminoethyl diphenylborinate (2-APB), Tetrahydrocannabivarin (THCV) and econazole have been reported to bind this site [26,65,80,81]. Additionally, two other major lipid binding sites, the shallow S4-S5 and the S1-S4 base, are primarily occupied by PI lipids across all six TRPVs. The shallow S4-S5 hosts econazole binding in TRPV6 (identical binding site to econazole in TRPV5, Fig. 6), while the S1-S4 base accommodates 2-APB in TRPV3 and TRPV6 [27,82], 9QM, X7N, XQ3, XPW, and XS9 in TRPV4 [83–86], and O6S in TRPV5 [87] (see Table S5 for the correspondences in ligand names and PDB ids). The overlap between lipid and ligand binding sites (representative cases in the insets in Fig. 6) reveals a critical dynamic—lipids can directly compete with or modulate drug binding, making them key players in the pharmacological landscape of membrane proteins and essential targets in drug discovery.

Besides, CHOL also binds to the upper vanilloid in TRPV3 and TRPV4. The large occupation of the vanilloid and upper vanilloid sites by CHOL may be attributed to its smaller size compared to the other lipids, allowing CHOL deeper insertion into the protein structure where larger lipid species cannot access. In contrast, bulkier lipids such as PAP1, and PAP6 preferentially occupy the S2-S3 site (except for TRPV2), likely due to steric constraints preventing them from accessing more

deeply buried cavities.

2.5.4.2. Drug-only binding sites. Interestingly, certain binding sites, including the selectivity filter, the intracellular pore entry, the deep portal and the shallow portal, that are occupied by ligands, have no lipids detected in our simulations. This may reflect the size and hydrophobicity barriers lipids face when attempting to access the pore region, compared to the ligands found in the pore (R2R, dyclonine, PCHPD3, PCHPD4), which already encounter challenges moving through the protein chains to reach the pore. Furthermore, lipids to access the pore would likely require fenestration from the bilayer, as observed in other ion channels [88], further limiting their entry compared to smaller, more soluble ligands.

In fact, the lack of lipids in known drug binding sites can be related to one of the main limitations in this study. While the Martini CG force field has proven highly valuable for exploring LPI at microsecond timescales, the use of an elastic network to preserve protein secondary and tertiary structure introduces conformational limitations [89]. In this regard, the application of harmonic restraints limits the sampling of large-scale motions, such as pore opening or gating transitions, and reduces the possibilities of a lipid binding in deeper binding sites, which biases the identification of binding sites to those only accessible in specific functional states.

Nevertheless, the use of CG-MD also offers some advantages compared to experimental studies. While some lipid-protein interactions are very stable and can remain bound for the time and conditions of the purification and structural determination process, most are more transient, although biologically relevant. In this regard, CG-MD allows to expose the protein to a complex membrane composition and gain insights on where each lipid interacts with each channel. Moreover, computational studies (especially CG studies) allow to use complex membrane compositions, closer to the actual cell membrane composition, which can lead to discover new lipid bindings in drug binding sites, and even novel binding sites within the protein core.

2.5.4.3. “Orphan” lipid binding sites. Various binding sites where lipids bind stably have been found, yet no ligands have been described to date. One interpretation for these results is that lipids may be uniquely capable of stabilizing certain sites that are less accessible or less favorable for drug-like molecules. Notably, the newly defined lipid binding sites have yet to be characterized biochemically and functionally and, so far, structural biology has not resolved any drug bound to these sites. This raises the possibility of exploring the druggability of such cavities and highlights the potential opportunities for structure/fragment-based drug discovery strategies to compete with these bioactive lipids.

3. Conclusions

CG-MD simulations overcome the time scale limitations associated with lipid diffusion, as previously demonstrated for lipid fingerprinting. In this study, the time scale used is shorter compared to other studies, but replicates show convergence. The four-fold symmetry of TRPVs enhances sampling, justifying the shorter time and making it more accessible to labs with modest computational equipment. This makes the CG-MD lipid fingerprinting method suitable for routine computational biophysics discovery and screening strategies due to its computational efficiency, ability to study large systems and complex membrane compositions, conferring potential to uncover new lipid-protein interactions.

However, some limitations must be considered to accurately interpret these results. Accurate parameterization of the force field and possible biases derived from inaccuracies in the model are a common concern in any MD simulation. In addition, the Martini force field allows an increased sampling by reducing atomic detail, which highlights the importance of our structural cross-validation and the need for further experimental work.

The functional paralipidome may vary with the conformational state of membrane proteins. Our approach combines the Martini force field with an elastic network, a common strategy to compensate for the lack of hydrogen bonding in the model. However, the presence of elastic network impedes any significant changes in secondary and tertiary structure. In the case of TRPVs, gating-derived conformational dynamics cannot be observed using our approach. Therefore, the paralipidome of TRPVs could be more dynamic and intricate than the one here presented.

Nonetheless, our study corroborates lipid binding biochemical and structural biology studies on the TRPV subfamily, also revealing new intricate lipid-protein interactions relevant for TRPV physiology. The method complements structural biology, as protein isolation often involves removing them from their native environment, potentially introducing biases in lipid composition and the lipids attached to the final structures. Altering membrane composition can change the collective properties of the membrane. Simulations can mitigate this bias by incorporating more complex lipid mixtures and, specifically, CG-MD lipid fingerprinting can aid dubious lipid densities assignment in membrane proteins structural biology.

This methodology can help in understanding the physio-pathological implications for each channel, as well as to correlate lipid affinities with drug pharmacology. In general terms, the approach presented here opens up exciting opportunities for developing lipid-based targeted therapies and discovering novel druggable sites in key targets, such as membrane proteins, paving the way towards more efficient and versatile drug design and discovery strategies.

4. Methods

4.1. Simulation details

4.1.1. System setup

The starting coordinates of each TRPV channel were downloaded from the Protein Data Bank (PDB ids in Table 3) and converted to Martini 2.2 CG force field using the *martinize.py* script applying an elastic network on atom pairs within a 0.9 nm cut-off with a 500 kJ

Table 3

PDB code of the TRPV structures used.

Channel	TRPV1	TRPV2	TRPV3	TRPV4	TRPV5	TRPV6
PDB code	8GF8	6U84	6MHO	8T1B	6O1P	6BOB

$\text{mol}^{-1} \text{nm}^{-2}$ force constant [89,90]. After that, the CG protein was embedded in an asymmetric complex lipid bilayer containing approximately 1500 lipids on each leaflet (Table S1, Table S2) using the program *insane.py* [91]. The composition of the lipid membrane was based on the plasma membrane model previously described by Ingólfsson et al. [28], with minor modifications (Table 1). Each system was solvated in CG water and neutralized with Na^+ and Cl^- ions to a final concentration of 0.15 M (total number of waters, ions and protein beads is in Table 4). Lipid topology files were obtained from the Martini repository and PAP6 was obtained from Ingólfsson et al. [92]

4.1.2. Simulation setup

Simulations were carried out with the GROMACS simulation package version 2020 [93–98]. An initial two-step energy minimization (5000 steps each) was performed using the steepest descent algorithm with soft-core and standards hard-core potentials, respectively. A 4.75 ns equilibration divided in 5 steps was run in the NPT ensemble with decreasing positional restraints in lipid heads (1000, 500, 250, 100, and 50 $\text{kJ}\cdot\text{mol}^{-1}$, respectively) and protein backbone beads (200, 100, 50, 20, 10 $\text{kJ}\cdot\text{mol}^{-1}$, respectively) and increasing integration steps (1, 5, 10, 15, and 20 fs, respectively). Finally, a production run with no restraints was run for 5 μs for each system with a 20-fs time step. Each system (TRPV) was simulated three independent times.

Temperature was maintained at 310.15 K using the V-rescale thermostat, and a semi-isotropic 1 bar pressure was maintained using the Berendsen (equilibration steps) or Parrinello-Rahman (production run) barostats. Periodic boundary conditions and the reaction field method were used to account for long-range electrostatics, applying a cutoff of 1.1 nm and a relative permittivity of $\epsilon_r = 15$. For the Leonard-Jones terms, a potential-shift with the Verlet cutoff-scheme with a value of 1.1 nm for the cutoff was applied.

4.2. Data analysis

4.2.1. Trajectory analysis

Trajectories were centered on the protein using the GROMACS built-in *gmx trjconv* tool. For each replicate, one frame was saved for each nanosecond (5000 frames per trajectory) of simulation and used for the data analysis.

Table 4

Details on each system composition of water, ion, and total number of beads.

Channel	Replica	Water beads	Ions (Na/Cl)	Total number of beads
TRPV1	1	141,011	1960/1557	182,741
	2	140,900	1960/1557	182,720
	3	140,970	1959/1556	182,698
TRPV2	1	140,564	1954/1552	182,716
	2	140,512	1953/1551	182,662
	3	140,553	1954/1552	182,705
TRPV3	1	140,780	1981/1555	182,482
	2	140,744	1980/1554	182,444
	3	140,764	1980/1554	182,464
TRPV4	1	140,746	1947/1554	182,794
	2	140,733	1947/1554	182,781
	3	140,776	1947/1554	182,824
TRPV5	1	140,683	1989/1554	182,143
	2	140,676	1989/1554	182,136
	3	140,691	1989/1554	182,151
TRPV6	1	141,921	1983/1567	183,521
	2	141,918	1983/1567	183,518
	3	141,918	1983/1567	183,518

4.2.2. Initial vs final lipid microenvironment

The lipid depletion/enrichment around the protein was measured by comparing the initial lipid composition of the membrane and the composition of the lipids around the protein during the last 500 ns across all 3 replicates. Briefly, a lipid was considered to be in contact with the protein if any of its beads were at a distance of 5.5 Å or lower. The total number of each individual lipid in contact with the protein over the combined 500 ns of the three replicates was normalized by the total amount of all lipids that the protein has been in contact to calculate the final lipid microenvironment composition as percentage of each lipid (Eq. (1)) [99]:

$$DE_x = \frac{L_{x(0.55)} / L_{T(0.55)}}{L_{x(\text{membrane})} / L_{T(\text{membrane})}} \quad (1)$$

Where DE is the depletion-enrichment index, L is the number of lipids for a given lipid species X or for any lipid type (T) in the mixture around 0.55 nm of any TRPV residue or in the whole membrane.

4.2.3. Lipid occupancy and residence time and prediction of binding events

Calculation of residue occupancy/residence time and prediction of potential lipid binding events was performed with PyLipID using a dual cut-off of 0.475–0.7 nm (lower and higher cut-offs, respectively), as previously described [99,100].

Briefly, PyLipID calculates occupancy as the fraction of frames in which a given residue is in contact with the selected lipid species. Residence time is computed in a multi-step process: firstly, for each residue-lipid pair, a survival time correlation function ((t)) is calculated and normalized so $(0) = 1$. This function is then fitted to a bi-exponential decay model to extract the dissociation rate constant (k_{off}), from which the residence time (τ) is obtained as its inverse ($\tau = 1/k_{off}$).

For binding event detection, PyLipID identifies groups of residues interacting at the same time with a given lipid molecule. This is achieved by creating a Pearson Correlation matrix based on the distances of each residue to the lipid molecule. The resulting matrix is used to build a weighted network in which the nodes are the residues, and the edges represent the correlation coefficients. The matrix is finally decomposed into communities using the Louvain algorithm [101]. Only communities with at least 4 residues/nodes were considered potential binding events.

4.2.4. Weighted GRAVY score binding region analysis

The GRAVY score of each binding event is defined as the weighted average of the hydrophobicity values, as determined from Kyte-Doolittle [102], of each residue involved in the binding (Eq. (2)):

$$\text{GRAVY score} = \frac{1}{n} \sum HI_{aa} \cdot \text{restime}_{aa} \quad (2)$$

Where aa is the corresponding residue in the binding pocket of the binding event, HI is the Kyte-Doolittle hydrophobicity index of that residue, restime is its residence time (as calculated by PyLipID), and n is the total number of residues involved in the event.

4.2.5. Residue conservation

The conservation of each residue was calculated using ConSurf conservation score [70–75]. The conservation score is based on the sequence similarity computed on a multiple sequence alignment based on a dataset of available structures and sequences for TRPV proteins (Fig. S4). The conservation score of the binding sites was calculated by averaging the conservation value of all the residues implicated in the binding.

4.2.6. Molecular representation

To generate Fig. 6, all TRPV Cryo-EM structures found in the PDB database [103] were manually curated to remove lipids, ions, waters, and additives. All figures and molecular representation have been

generated using VMD [104].

CRediT authorship contribution statement

Mario Lopez-Martin: Writing – original draft, Supervision, Methodology, Investigation, Formal analysis, Conceptualization. **Eric Cataлина-Hernandez:** Writing – review & editing, Writing – original draft, Visualization, Methodology, Investigation, Formal analysis, Data curation. **Alex Peralvarez-Marin:** Writing – review & editing, Writing – original draft, Supervision, Resources, Methodology, Investigation, Funding acquisition, Formal analysis, Conceptualization.

Declaration of competing interest

The authors declare that they have no known competing financial interests or personal relationships that could have appeared to influence the work reported in this paper.

Acknowledgements

We thank Prof. Peter D. Tielemans for critical reading of the manuscript. Authors acknowledge financial support by the Spanish Government Grant PID2020-120222GB-I00 (to A.P.-M.) funded by MCIN/AEI/10.13039/501100011033, Ministerio de Universidades Margarita Salas Award (MGSD2021-10 to M.L.-M.) and Universitat Autònoma de Barcelona predoctoral fellowship (B21P0033 to E.C.-H.).

Appendix A. Supplementary data

Supplementary data to this article can be found online at <https://doi.org/10.1016/j.ijbiomac.2025.148108>.

Data availability

A GitHub repository (https://github.com/APMlab-memb/TRPVs_Paralipidome.git) has been made available containing the systems initial structure, the lipid topology files, and the analysis scripts. Trajectories will be made available upon request.

References

- [1] S.J. Singer, G.L. Nicolson, The fluid mosaic model of the structure of cell membranes, *Science* (1979) 175 (4023) (1972) 720–731, <https://doi.org/10.1126/SCIENCE.175.4023.720>.
- [2] S.J. Wodak, S. Velankar, Structural biology: the transformational era, *Proteomics* 23 (17) (2023) 2200084, <https://doi.org/10.1002/PMIC.202200084>.
- [3] M. Overduin, C. Trieber, R.S. Prosser, L.P. Picard, J.G. Sheff, Structures and dynamics of native-state transmembrane protein targets and bound lipids, *Membranes* 11 (6) (2021) 451, <https://doi.org/10.3390/MEMBRANES11060451>.
- [4] I. Levental, E. Lyman, Regulation of membrane protein structure and function by their lipid nano-environment, *Nat. Rev. Mol. Cell Biol.* 24 (2) (2022) 107–122, <https://doi.org/10.1038/s41580-022-00524-4>.
- [5] T.B. Ansell, W. Song, C.E. Coupland, L. Carriqué, R.A. Corey, A.L. Duncan, C. K. Cassidy, M.M.G. Geurts, T. Rasmussen, A.B. Ward, C. Siebold, P.J. Stansfeld, M.S.P. Sansom, LipIDens: simulation assisted interpretation of lipid densities in Cryo-EM structures of membrane proteins, *Nat. Commun.* 14 (1) (2023), <https://doi.org/10.1038/s41467-023-43392-y>.
- [6] V. Corradi, E. Mendez-Villuendas, H.I. Ingólfsson, R.X. Gu, I. Siuda, M.N. Melo, A. Moussatova, L.J. Degagné, B.I. Sejdiu, G. Singh, T.A. Wassenaar, K. Delgado Magnero, S.J. Marrink, D.P. Tielemans, Lipid-protein interactions are unique fingerprints for membrane proteins, *ACS Cent. Sci.* 4 (6) (2018) 709–717, <https://doi.org/10.1021/ACSCENTSCI.8B00143>.
- [7] C. Bergh, U. Rovničnik, R. Howard, E. Lindahl, Discovery of lipid binding sites in a ligand-gated ion channel by integrating simulations and Cryo-EM, *Elife* (2024) 13, <https://doi.org/10.7554/ELIFE.86016>.
- [8] B. Nilius, G. Owsianik, The transient receptor potential family of ion channels, *Genome Biol.* 12 (3) (2011) 1–11, <https://doi.org/10.1186/GB-2011-12-3-218>.
- [9] S.F. Pedersen, G. Owsianik, B. Nilius, TRP channels: an overview, *Cell Calcium* 38 (3–4) (2005) 233–252, <https://doi.org/10.1016/J.CECA.2005.06.028>.
- [10] B. Nilius, R. Vennekens, G. Owsianik, Vanilloid transient receptor potential cation channels: an overview, *Curr. Pharm. Des.* 14 (1) (2008) 18–31, <https://doi.org/10.2174/138161208783330763>.

- [11] R.L. Baylie, J.E. Brayden, TRPV channels and vascular function, *Acta Physiol.* 203 (1) (2011) 99–116, <https://doi.org/10.1111/J.1748-1716.2010.02217.X>.
- [12] H. Lee, M.J. Caterina, TRPV channels as thermosensory receptors in epithelial cells, *Pflugers Arch.* 451 (1) (2005) 160–167, <https://doi.org/10.1007/S00424-005-1438-Y>.
- [13] P. Geppetti, S. Materazzi, P. Nicoletti, The transient receptor potential Vanilloid 1: role in airway inflammation and disease, *Eur. J. Pharmacol.* 533 (1–3) (2006) 207–214, <https://doi.org/10.1016/J.EJP.2005.12.063>.
- [14] M. Tominaga, T. Tominaga, Structure and function of TRPV1, *Pflugers Arch.* 451 (1) (2005) 143–150, <https://doi.org/10.1007/S00424-005-1457-8>.
- [15] C. Liu, L. Xue, C. Song, Calcium binding and permeation in TRPV channels: insights from molecular dynamics simulations, *J. Gen. Physiol.* 155 (12) (2023) e202213261, <https://doi.org/10.1085/jgp.202213261>.
- [16] C.D. Benham, M.J. Gunthorpe, J.B. Davis, TRPV channels as temperature sensors, *Cell Calcium* 33 (5–6) (2003) 479–487, [https://doi.org/10.1016/S0143-4160\(03\)00063-0](https://doi.org/10.1016/S0143-4160(03)00063-0).
- [17] R.G. O’Neil, S. Heller, The mechanosensitive nature of TRPV channels, *Pflugers Arch.* 451 (1) (2005) 193–203, <https://doi.org/10.1007/S00424-005-1424-4>.
- [18] J.-B. Peng, Y. Suzuki, G. Gyimesi, M.A. Hediger, TRPV5 and TRPV6 calcium-selective channels, *Calcium Entry Chan. Non-Excitable Cells* (2017) 241–274, <https://doi.org/10.1201/978131512592-13>.
- [19] M. Van Abel, J.G.J. Hoenderop, R.J.M. Bindels, The epithelial calcium channels TRPV5 and TRPV6: regulation and implications for disease, *Naunyn Schmiedeberg’s Arch. Pharmacol.* 371 (4) (2005) 295–306, <https://doi.org/10.1007/S00210-005-1021-2>.
- [20] M. Liao, E. Cao, D. Julius, Y. Cheng, Structure of the TRPV1 ion channel determined by electron cryo-microscopy, *Nature* 504 (7478) (2013) 107–112, <https://doi.org/10.1038/nature12822>.
- [21] B.A. Niemeyer, Structure-function analysis of TRPV channels, *Naunyn Schmiedeberg’s Arch. Pharmacol.* 371 (4) (2005) 285–294, <https://doi.org/10.1007/S00210-005-1053-7>.
- [22] M.Y. Song, J.X.J. Yuan, Introduction to TRP channels: structure, function, and regulation, *Adv. Exp. Med. Biol.* 661 (2010) 99–108, https://doi.org/10.1007/978-1-60761-500-2_6.
- [23] M. Li, Y. Yu, J. Yang, Structural biology of TRP channels, *Adv. Exp. Med. Biol.* 704 (2011) 1–23, https://doi.org/10.1007/978-94-007-0265-3_1.
- [24] S.L. Morales-Lázaro, L. Lemus, T. Rosenbaum, Regulation of ThermoTRPs by lipids, *Temperature* 4 (1) (2017) 24–40, <https://doi.org/10.1080/23328940.2016.1254136>.
- [25] A. Rosenhouse-Dantsker, D. Mehta, I. Levitan, Regulation of ion channels by membrane lipids, *Compr. Physiol.* 2 (1) (2012) 31–68, <https://doi.org/10.1002/CYH.C11001>.
- [26] N. Su, W. Zhen, H. Zhang, L. Xu, Y. Jin, X. Chen, C. Zhao, Q. Wang, X. Wang, S. Li, H. Wen, W. Yang, J. Guo, F. Yang, Structural mechanisms of TRPV2 modulation by endogenous and exogenous ligands, *Nat. Chem. Biol.* 19 (1) (2023) 72–80, <https://doi.org/10.1038/s41589-022-01139-8>.
- [27] A.K. Singh, K. Saotome, L.L. McGoldrick, A.I. Sobolevsky, Structural bases of TRP channel TRPV6 allosteric modulation by 2-APB, *Nat. Commun.* 9 (1) (2018) 1–11, <https://doi.org/10.1038/s41467-018-04828-y>.
- [28] H.I. Ingólfsson, H. Bhatia, T. Zeppelin, W.F.D. Bennett, K.A. Carpenter, P.C. Hsu, G. Dharuman, P.T. Bremer, B. Schiøtt, F.C. Lightstone, T.S. Carpenter, Capturing biologically complex tissue-specific membranes at different levels of compositional complexity, *J. Phys. Chem. B* 124 (36) (2020) 7819–7829, <https://doi.org/10.1021/ACS.JPCB.0C03368>.
- [29] H.I. Ingólfsson, M.N. Melo, F.J. Van Eerdent, C. Arnarez, C.A. Lopez, T. A. Wassenaar, X. Periore, A.H. De Vries, D.P. Tielemans, S.J. Marrink, Lipid organization of the plasma membrane, *J. Am. Chem. Soc.* 136 (41) (2014) 14554–14559, <https://doi.org/10.1021/JA507832E>.
- [30] P. Donáte-Macíán, E. Álvarez-Marimon, F. Sepulcre, J.L. Vázquez-Ibar, A. Perálvarez-Marín, The membrane proximal domain of TRPV1 and TRPV2 channels mediates protein–protein interactions and lipid binding in vitro, *Int. J. Mol. Sci.* 20 (3) (2019), <https://doi.org/10.3390/ijms20030682>.
- [31] S.L. Morales-Lázaro, I. Llorente, F. Sierra-Ramírez, A.E. López-Romero, M. Ortíz-Rentería, B. Serrano-Flores, S.A. Simon, L.D. Islas, T. Rosenbaum, Inhibition of TRPV1 channels by a naturally occurring omega-9 fatty acid reduces pain and itch, *Nat. Commun.* 7 (1) (2016) 1–12, <https://doi.org/10.1038/ncomms13092>.
- [32] S.L. Morales-Lázaro, T. Rosenbaum, A painful link between the TRPV1 channel and lysophosphatidic acid, *Life Sci.* 125 (2015) 15–24, <https://doi.org/10.1016/J.LS.2014.10.004>.
- [33] A. Nieto-Posadas, G. Picazo-Juárez, I. Llorente, A. Jara-Oseguera, S. Morales-Lázaro, D. Escalante-Alcalde, L.D. Islas, T. Rosenbaum, Lysophosphatidic acid directly activates TRPV1 through a C-Terminal binding site, *Nat. Chem. Biol.* 8 (1) (2011) 78–85, <https://doi.org/10.1038/nchembio.712>.
- [34] S. Feng, R.A. Pumroy, A.D. Protopopova, V.Y. Moiseenkova-Bell, W. Im, Modulation of TRPV2 by endogenous and exogenous ligands: a computational study, *Protein Sci.* 32 (1) (2023) e4490, <https://doi.org/10.1002/pro.4490>.
- [35] T. Rohacs, B. Nilius, Regulation of Transient Receptor Potential (TRP) channels by phosphoinositides, *Pflugers Arch. - Eur. J. Physiol.* 455 (1) (2007) 157–168, <https://doi.org/10.1007/S00424-007-0275-6>.
- [36] B. Liu, C. Zhang, F. Qin, Functional recovery from desensitization of Vanilloid receptor TRPV1 requires resynthesis of phosphatidylinositol 4,5-bisphosphate, *J. Neurosci.* 25 (19) (2005) 4835–4843, <https://doi.org/10.1523/JNEUROSCI.1296-05.2005>.
- [37] A. Garcia-Elias, S. Mrkonjić, C. Pardo-Pastor, H. Inada, U.A. Hellmich, F. Rubio-Moscárdó, C. Plata, R. Gaudet, R. Vicente, M.A. Valverde, Phosphatidylinositol-4,5-Biphosphate-dependent rearrangement of TRPV4 cytosolic tails enables channel activation by physiological stimuli, *Proc. Natl. Acad. Sci. USA* 110 (23) (2013) 9553–9558, <https://doi.org/10.1073/PNAS.1220231110>.
- [38] L.I. Horvath, P.J. Brophy, D. Marsh, Exchange rates at the lipid–protein interface of myelin proteolipid protein studied by spin-label electron spin resonance, *Biochemistry* 27 (1) (1988) 46–52, <https://doi.org/10.1021/B100401A009>.
- [39] A. Buyan, C.D. Cox, J. Barnoud, J. Li, H.S.M. Chan, B. Martinac, S.J. Marrink, B. Corry, Piezo1 forms specific, functionally important interactions with phosphoinositides and cholesterol, *Biophys. J.* 119 (8) (2020) 1683, <https://doi.org/10.1016/J.BPJ.2020.07.043>.
- [40] M.R. Schmidt, P.J. Stansfeld, S.J. Tucker, M.S.P. Sansom, Simulation-based prediction of phosphatidylinositol 4,5-bisphosphate binding to an ion channel, *Biochemistry* 52 (2) (2013) 279–281, <https://doi.org/10.1021/B13013508>.
- [41] R.V. Stahelin, J.L. Scott, C.T. Frick, Cellular and molecular interactions of phosphoinositides and peripheral proteins, *Chem. Phys. Lipids* 182 (2014) 3–18, <https://doi.org/10.1016/J.CHEMPHYSLIP.2014.02.002>.
- [42] P. Donáte-Macíán, Identification and Characterization of the TRPVs Protein-Protein Interactions, a Comprehensive Approach to Elucidate TRPVs Function and Regulation, *Universitat Autònoma de Barcelona*, 2016.
- [43] J.L. Symons, K.J. Cho, J.T. Chang, G. Du, M.N. Waxham, J.F. Hancock, I. Levental, K.R. Levental, Lipidomic atlas of mammalian cell membranes reveals hierarchical variation induced by culture conditions, subcellular membranes, and cell lineages, *Soft Matter* 17 (2) (2021) 288–297, <https://doi.org/10.1039/DOM00404A>.
- [44] M. Lakk, G.F. Hoffmann, A. Gorusupudi, E. Enyong, A. Lin, P.S. Bernstein, T. Toft-Bertelsen, N. MacAulay, M.H. Elliott, D. Križaj, Membrane cholesterol regulates TRPV4 function, cytoskeletal expression, and the cellular response to tension, *J. Lipid Res.* 62 (2021) 100145–100146, <https://doi.org/10.1016/J.JLR.2021.100145>.
- [45] E. Fahy, S. Subramaniam, H.A. Brown, C.K. Glass, A.H. Merrill, R.C. Murphy, C.R. H. Raetz, D.W. Russell, Y. Seyama, W. Shaw, T. Shimizu, F. Spener, G. Van Meer, M.S. VanNieuwenhze, S.H. White, J.L. Witztum, E.A. Dennis, A comprehensive classification system for lipids, *J. Lipid Res.* 46 (5) (2005) 839–861, <https://doi.org/10.1194/JLR.E400004-JLR200>.
- [46] C. Wu, M. Sun, M. Qile, Y. Zhang, L. Liu, X. Cheng, X. Dai, E.R. Gross, Y. Zhang, S. He, Lysophosphatidic acid contributes to myocardial ischemia/reperfusion injury by activating TRPV1 in spinal cord, *Basic Res. Cardiol.* 119 (2) (2024) 329–348, <https://doi.org/10.1007/S00395-023-01031-Z>.
- [47] M. Benítez-Angeles, A.E.L. Romero, I. Llorente, I. Hernández-Araiza, A. Vergara-Jaque, F.H. Real, O.E. Gutiérrez-Castañeda, M. Arciniega, L.E. Morales-Buenrostro, F. Torres-Quirolo, R. García-Villegas, L.B. Tovar-y-Romo, W. B. Liedtke, L.D. Islas, T. Rosenbaum, Modes of action of lysophospholipids as endogenous activators of the TRPV4 ion channel, *J. Physiol.* 601 (9) (2023) 1655–1673, <https://doi.org/10.1113/JP284262>.
- [48] T. Rohacs, Phosphoinositide regulation of TRP channels: a functional overview in the structural era, *Annu. Rev. Physiol.* 86 (Volume 86, 2024) (2024) 329–355, <https://doi.org/10.1146/ANNUREV-PHYSIOL-042022-013956>.
- [49] S. Standoli, S. Pecchioli, D. Tortolani, C. Di Meo, F. Fanti, M. Sergi, M. Bacci, I. Seidita, C. Bernacchioni, C. Donati, P. Bruni, M. Maccarrone, C. Rapino, F. Cencetti, The TRPV1 receptor is up-regulated by Sphingosine 1-phosphate and is implicated in the anandamide-dependent regulation of mitochondrial activity in C2C12 myoblasts, *Int. J. Mol. Sci.* 23 (19) (2022) 11103, <https://doi.org/10.3390/IJMS23191103>.
- [50] É. Sághy, É. Szoke, M. Payrits, Z. Helyes, R. Börzsei, J. Erostýák, T.Z. Jánosi, G. Sétálo, J. Szolcsányi, Evidence for the role of lipid rafts and sphingomyelin in Ca²⁺-gating of transient receptor potential channels in trigeminal sensory neurons and peripheral nerve terminals, *Pharmacol. Res.* 100 (2015) 101–116, <https://doi.org/10.1016/J.PHRNS.2015.07.028>.
- [51] G. Von Heijne, Membrane-protein topology, *Nat. Rev. Mol. Cell Biol.* 7 (12) (2006) 909–918, <https://doi.org/10.1038/nrm2063>.
- [52] G. VonHeijne, Control of topology and mode of assembly of a polytopic membrane protein by positively charged residues, *Nature* 341 (6241) (1989) 456–458, <https://doi.org/10.1038/341456a0>.
- [53] V. Lukacs, J.M. Rives, X. Sun, E. Zakharian, T. Rohacs, Promiscuous activation of Transient Receptor Potential Vanilloid 1 (TRPV1) channels by negatively charged intracellular lipids, *J. Biol. Chem.* 288 (49) (2013) 35003–35013, <https://doi.org/10.1074/JBC.M113.520288>.
- [54] S. Kumari, A. Kumar, P. Sardar, M. Yadav, R.K. Majhi, A. Kumar, C. Goswami, Influence of membrane cholesterol in the molecular evolution and functional regulation of TRPV4, *Biochem. Biophys. Res. Commun.* 456 (1) (2015) 312–319, <https://doi.org/10.1016/J.BBRC.2014.11.077>.
- [55] A.S. Klein, A. Tannert, M. Schaefer, Cholesterol Sensitises the transient receptor potential channel TRPV3 to lower temperatures and activator concentrations, *Cell Calcium* 55 (1) (2014) 59–68, <https://doi.org/10.1016/J.CECA.2013.12.001>.
- [56] S.L. Morales-Lázaro, T. Rosenbaum, Cholesterol as a key molecule that regulates TRPV1 channel function, *Adv. Exp. Med. Biol.* 1135 (2019) 105–117, https://doi.org/10.1007/978-3-030-14265-0_6.

- [57] E.T. Jansson, C.L. Trkulja, A. Ahemaiti, M. Millingen, G.D.M. Jeffries, K. Jardemark, O. Orwar, Effect of cholesterol depletion on the pore dilation of TRPV1, *Mol. Pain* 9 (1) (2013), <https://doi.org/10.1186/1744-8069-9-1>.
- [58] L. Kever, A. Cherezova, V. Zenin, Y. Negulyaev, Y. Komissarchik, S. Semenova, Downregulation of TRPV6 channel activity by cholesterol depletion in Jurkat T cell line, *Cell Biol. Int.* 43 (8) (2019) 965–975, <https://doi.org/10.1002/CB.11185>.
- [59] L.V. Kever, S.B. Semenova, The role of cholesterol in membrane localization of TRPV5 calcium channels in Jurkat human T cells, *Cell Tissue Biol.* 14 (4) (2020) 309–315, <https://doi.org/10.1134/S1990519X20040033>.
- [60] M. Manchanda, E. Leishman, K. Sangani, A. Alamri, H.B. Bradshaw, Activation of TRPV1 by capsaicin or heat drives changes in 2-Acyl glycerols and N-Acyl ethanolamines in time, dose, and temperature dependent manner, *Front. Cell Dev. Biol.* 9 (2021) 611952, <https://doi.org/10.3389/FCELL.2021.611952>.
- [61] H. Belrhali, P. Nollert, A. Royant, C. Menzel, J.P. Rosenbusch, E.M. Landau, E. Pebay-Peyroula, Protein, lipid and water organization in Bacteriorhodopsin crystals: a molecular view of the purple membrane at 1.9 Å resolution, *Structure* 7 (8) (1999) 909–917, [https://doi.org/10.1016/S0969-2126\(99\)80118-X](https://doi.org/10.1016/S0969-2126(99)80118-X).
- [62] K.E. McAuley, P.K. Fyfe, J.P. Ridge, N.W. Isaacs, R.J. Cogdell, M.R. Jones, Structural details of an interaction between Cardiolipin and an integral membrane protein, *Proc. Natl. Acad. Sci. USA* 96 (26) (1999) 14706–14711, <https://doi.org/10.1073/PNAS.96.26.14706>.
- [63] M.V. Yelshanskaya, A.I. Sobolevsky, Ligand-binding sites in Vanilloid-subtype TRP channels, *Front. Pharmacol.* 13 (2022), <https://doi.org/10.3389/fphar.2022.900623>.
- [64] Y. Gao, E. Cao, D. Julius, Y. Cheng, TRPV1 structures in nanodiscs reveal mechanisms of ligand and lipid action, *Nature* 534 (7607) (2016) 347–351, <https://doi.org/10.1038/nature17964>.
- [65] D.H. Kwon, F. Zhang, Y. Suo, J. Bouvette, M.J. Borgnia, S.Y. Lee, Heat-dependent opening of TRPV1 in the presence of capsaicin, *Nat. Struct. Mol. Biol.* 28 (7) (2021) 554–563, <https://doi.org/10.1038/s41594-021-00616-3>.
- [66] K. Zhang, D. Julius, Y. Cheng, Structural snapshots of TRPV1 reveal mechanism of poly-modal functionality, *Cell* 184 (20) (2021) 5138–5150.e12, <https://doi.org/10.1016/J.CELL.2021.08.012>.
- [67] K.D. Nadezhdin, A. Neuberger, Y.A. Trofimov, N.A. Krylov, V. Sinica, N. Kupko, V. Vlachova, E. Zakharian, R.G. Efremov, A.I. Sobolevsky, Structural mechanism of heat-induced opening of a temperature-sensitive TRP channel, *Nat. Struct. Mol. Biol.* 28 (7) (2021) 564–572, <https://doi.org/10.1038/s41594-021-00615-4>.
- [68] T.E.T. Hughes, R.A. Pumroy, A.T. Yazici, M.A. Kasimova, E.C. Fluck, K.W. Huynh, A. Samanta, S.K. Molugu, Z.H. Zhou, V. Carnevale, T. Rohacs, V.Y. Moiseenkova-Bell, Structural insights on TRPV5 gating by endogenous modulators, *Nat. Commun.* 9 (1) (2018) 4198, <https://doi.org/10.1038/s41467-018-06753-6>.
- [69] A. Berna-Erro, M. Izquierdo-Serra, R.V. Sepúlveda, F. Rubio-Moscardo, P. Donaté-Macián, S.A. Serra, J. Carrillo-García, A. Perálvarez-Marín, F. González-Nilo, J. M. Fernández-Fernández, M.A. Valverde, Structural determinants of 5',6'-Epoxyeicosatrienoic acid binding to and activation of TRPV4 channel, *Sci. Rep.* 7 (1) (2017), <https://doi.org/10.1038/s41598-017-11274-1>.
- [70] F. Glaser, T. Pupko, I. Paz, R.E. Bell, D. Bechor-Shental, E. Martz, N. Ben-Tal, ConSurf: identification of functional regions in proteins by surface-mapping of phylogenetic information, *Bioinformatics* 19 (1) (2003) 163–164, <https://doi.org/10.1093/BIOINFORMATICS/19.1.163>.
- [71] M. Landau, I. Mayrose, Y. Rosenberg, F. Glaser, E. Martz, T. Pupko, N. Ben-Tal, ConSurf 2005: the projection of evolutionary conservation scores of residues on protein structures, *Nucleic Acids Res.* 33 (suppl_2) (2005) W299–W302, <https://doi.org/10.1093/NAR/GKI370>.
- [72] H. Ashkenazy, E. Erez, E. Martz, T. Pupko, N. Ben-Tal, ConSurf 2010: calculating evolutionary conservation in sequence and structure of proteins and nucleic acids, *Nucleic Acids Res.* 38 (suppl_2) (2010) W529–W533, <https://doi.org/10.1093/NAR/GKQ399>.
- [73] G. Celniker, G. Nimrod, H. Ashkenazy, F. Glaser, E. Martz, I. Mayrose, T. Pupko, N. Ben-Tal, Consurf: using evolutionary data to raise testable hypotheses about protein function, *Isr. J. Chem.* 53 (3–4) (2013) 199–206, <https://doi.org/10.1002/IJCH.20120096>.
- [74] H. Ashkenazy, S. Abadi, E. Martz, O. Chay, I. Mayrose, T. Pupko, N. Ben-Tal, ConSurf 2016: an improved methodology to estimate and visualize evolutionary conservation in macromolecules, *Nucleic Acids Res.* 44 (W1) (2016) W344–W350, <https://doi.org/10.1093/NAR/GKW408>.
- [75] B. Yariv, E. Yariv, A. Kessel, G. Masrati, A. Ben Chorin, E. Martz, I. Mayrose, T. Pupko, N. Ben-Tal, Using evolutionary data to make sense of macromolecules with a “face-lifted” ConSurf, *Protein Sci.* 32 (3) (2023) e4582, <https://doi.org/10.1002/PRO.4582>.
- [76] U.A. Hellmich, R. Gaudet, Structural biology of TRP channels, *Handb. Exp. Pharmacol.* 223 (2014) 963–990, https://doi.org/10.1007/978-3-319-05161-1_10.
- [77] È. Catalina-Hernández, M. López-Martín, D. Masnou-Sánchez, M. Martins, V. A. Lorenz-Fonfria, F. Jiménez-Altyó, U.A. Hellmich, H. Inada, A. Alcaraz, Y. Furutani, A. Nonell-Canals, J.L. Vázquez-Ibar, C. Domene, R. Gaudet, A. Perálvarez-Marín, Experimental and computational biophysics to identify vasodilator drugs targeted at TRPV2 using agonists based on the probenecid scaffold, *Comput. Struct. Biotechnol. J.* 23 (2024) 473–482, <https://doi.org/10.1016/j.csbj.2023.12.028>.
- [78] J. Mercado, A. Gordon-Shaq, W.N. Zagotta, S.E. Gordon, Ca²⁺-dependent desensitization of TRPV2 channels is mediated by hydrolysis of phosphatidylinositol 4,5-bisphosphate, *J. Neurosci.* 30 (40) (2010) 13338–13347, <https://doi.org/10.1523/JNEUROSCI.2108-10.2010>.
- [79] J.F. Doerner, H. Hatt, I.S. Ramsey, Voltage- and temperature-dependent activation of TRPV3 channels is potentiated by receptor-mediated PI(4,5)P₂ hydrolysis, *J. Gen. Physiol.* 137 (3) (2011) 271–288, <https://doi.org/10.1085/JGP.200910388>.
- [80] K.D. Nadezhdin, A. Neuberger, L.S. Khosrof, I.A. Talyzina, J. Khau, M. V. Yelshanskaya, A.I. Sobolevsky, TRPV3 activation by different agonists accompanied by lipid dissociation from the Vanilloid site, *Sci. Adv.* 10 (18) (2024) 2453, <https://doi.org/10.1126/SCIADV.ADN2453>.
- [81] T.E.T. Hughes, D.T. Ladowski, K.W. Huynh, A. Yazici, J. Del Rosario, A. Kapoor, S. Basak, A. Samanta, X. Han, S. Chakrapani, Z.H. Zhou, M. Filizola, T. Rohacs, S. Han, V.Y. Moiseenkova-Bell, Structural basis of TRPV5 channel inhibition by econazole revealed by Cryo-EM, *Nat. Struct. Mol. Biol.* 25 (1) (2018) 53–60, <https://doi.org/10.1038/s41594-017-0009-1>.
- [82] A.K. Singh, L.L. McGoldrick, A.I. Sobolevsky, Structure and gating mechanism of the transient receptor potential channel TRPV3, *Nat. Struct. Mol. Biol.* 25 (9) (2018) 805–813, <https://doi.org/10.1038/s41594-018-0108-7>.
- [83] W. Zhen, Z. Zhao, S. Chang, X. Chen, Y. Wan, F. Yang, Structural basis of ligand activation and inhibition in a mammalian TRPV4 ion channel, *Cell Discov.* 9 (1) (2023) 70, <https://doi.org/10.1038/s41421-023-00579-3>.
- [84] K.D. Nadezhdin, I.A. Talyzina, A. Parthasarathy, A. Neuberger, D.X. Zhang, A. I. Sobolevsky, Structure of human TRPV4 in complex with GTPase RhoA, *Nat. Commun.* 14 (1) (2023) 1–11, <https://doi.org/10.1038/s41467-023-39346-z>.
- [85] D.H. Kwon, F. Zhang, B.A. McCray, S. Feng, M. Kumar, J.M. Sullivan, W. Im, C. J. Sumner, S.Y. Lee, TRPV4-Rho GTPase complex structures reveal mechanisms of gating and disease, *Nat. Commun.* 14 (1) (2023) 1–15, <https://doi.org/10.1038/s41467-023-39345-0>.
- [86] J. Fan, C. Guo, D. Liao, H. Ke, J. Lei, W. Xie, Y. Tang, M. Tominaga, Z. Huang, X. Lei, Structural pharmacology of TRPV4 antagonists, *Adv. Sci.* 11 (25) (2024) 2401583, <https://doi.org/10.1002/ADVS.202401583>.
- [87] T.E.T. Hughes, J.S. Del Rosario, A. Kapoor, A.T. Yazici, Y. Yudin, E.C. Fluck, M. Filizola, T. Rohacs, V.Y. Moiseenkova-Bell, Structure-based characterization of novel TRPV5 inhibitors, *Elife* 8 (2019), <https://doi.org/10.7554/ELIFE.49572>.
- [88] H.M. Frank, S. Walujkar, R.M. Walsh, W.J. Laursen, D.L. Theobald, P.A. Garrity, R. Gaudet, Structural basis of ligand specificity and channel activation in an insect gustatory receptor, *Cell Rep.* 43 (4) (2024) 114035, <https://doi.org/10.1016/J.CELREP.2024.114035>.
- [89] X. Periole, M. Cavalli, S.J. Marrink, M.A. Ceruso, Combining an elastic network with a coarse-grained molecular force field: structure, dynamics, and intermolecular recognition, *J. Chem. Theory Comput.* 5 (9) (2009) 2531–2543, <https://doi.org/10.1021/CT9002114>.
- [90] D.H. De Jong, G. Singh, W.F.D. Bennett, C. Arnarez, T.A. Wassenaar, L.V. Schäfer, X. Periole, D.P. Tielemans, S.J. Marrink, Improved parameters for the martini coarse-grained protein force field, *J. Chem. Theory Comput.* 9 (1) (2013) 687–697, <https://doi.org/10.1021/CT300646G>.
- [91] T.A. Wassenaar, H.I. Ingólfsson, R.A. Böckmann, D.P. Tielemans, S.J. Marrink, Computational lipidomics with insane: a versatile tool for generating custom membranes for molecular simulations, *J. Chem. Theory Comput.* 11 (5) (2015) 2144–2155, <https://doi.org/10.1021/ACS.JCTC.5B00209>.
- [92] H.I. Ingólfsson, C. Neale, T.S. Carpenter, R. Shrestha, C.A. Lopez, T.H. Tran, T. Oppelstrup, H. Bhatia, L.G. Stanton, X. Zhang, S. Sundram, F. Di Natale, A. Agarwal, G. Dharamani, S.I.L. Kokkila Schumacher, T. Turbyville, G. Gulten, Q. N. Van, D. Goswami, F. Jean-Francois, C. Agamasu, D. Chen, J.J. Hettige, T. Travers, S. Sarkar, M.P. Surh, Y. Yang, A. Moody, S. Liu, B.C. van Essen, A. F. Voter, A. Ramanathan, N.W. Hengartner, D.K. Simanshu, A.G. Stephen, P. T. Bremer, S. Gnanakaran, J.N. Glosli, F.C. Lightstone, F. McCormick, D. V. Nissley, F.H. Streitz, Machine learning-driven multiscale modeling reveals lipid-dependent dynamics of RAS signaling proteins, *Proc. Natl. Acad. Sci. USA* 119 (1) (2022) e2113297119, https://doi.org/10.1073/PNAS.2113297119/SUPPL_FILE/PNAS.2113297119.SAPP.PDF.
- [93] D. Van der Spoel, E. Lindahl, B. Hess, G. Groenhof, A.E. Mark, H.J.C. Berendsen, GROMACS: fast, flexible, and free, *J. Comput. Chem.* 26 (16) (2005) 1701–1718, <https://doi.org/10.1002/JCC.20291>.
- [94] H.J.C. Berendsen, D. van der Spoel, R. van Drunen, GROMACS: a message-passing parallel molecular dynamics implementation, *Comput. Phys. Commun.* 91 (1–3) (1995) 43–56, [https://doi.org/10.1016/0010-4655\(95\)00042-E](https://doi.org/10.1016/0010-4655(95)00042-E).
- [95] E. Lindahl, B. Hess, D. van der Spoel, GROMACS 3.0: a package for molecular simulation and trajectory analysis, *J. Mol. Model.* 7 (8) (2001) 306–317, <https://doi.org/10.1007/S008940100045/METRICS>.
- [96] M.J. Abraham, T. Murtola, R. Schulz, S. Páll, J.C. Smith, B. Hess, E. Lindahl, GROMACS: high performance molecular simulations through multi-level parallelism from laptops to supercomputers, *SoftwareX* 1–2 (2015) 19–25, <https://doi.org/10.1016/J.SOFTX.2015.06.001>.

- [97] B. Hess, C. Kutzner, D. Van Der Spoel, E. Lindahl, GROMACS 4: algorithms for highly efficient, load-balanced, and scalable molecular simulation, *J. Chem. Theory Comput.* 4 (3) (2008) 435–447, <https://doi.org/10.1021/CT700301Q>.
- [98] S. Pronk, S. Päll, R. Schulz, P. Larsson, P. Bjelkmar, R. Apostolov, M.R. Shirts, J. C. Smith, P.M. Kasson, D. Van Der Spoel, B. Hess, E. Lindahl, GROMACS 4.5: a high-throughput and highly parallel open source molecular simulation toolkit, *Bioinformatics* 29 (7) (2013) 845–854, <https://doi.org/10.1093/BIOINFORMATICS/BTT055>.
- [99] M. López-Martín, P. Renault, J. Giraldo, J.L. Vázquez-Ibar, A. Perálvarez-Marín, In silico assessment of the lipid fingerprint signature of ATP2, the essential P4-ATPase of malaria parasites, *Membranes (Basel)* 12 (7) (2022) 702, <https://doi.org/10.3390/MEMBRANES12070702/S1>.
- [100] W. Song, R.A. Corey, T.B. Ansell, C.K. Cassidy, M.R. Horrell, A.L. Duncan, P. J. Stansfeld, M.S.P. Sansom, Pylipid: a Python package for analysis of protein-lipid interactions from molecular dynamics simulations, *J. Chem. Theory Comput.* 18 (2) (2022) 1188–1201, <https://doi.org/10.1021/acs.jctc.1c00708>.
- [101] V.D. Blondel, J.-L. Guillaume, R. Lambiotte, E. Lefebvre, Fast unfolding of communities in large networks, *J. Stat. Mech.* (10) (2008), <https://doi.org/10.1088/1742-5468/2008/10/P10008>.
- [102] J. Kyte, R.F. Doolittle, A simple method for displaying the hydrophobic character of a protein, *J. Mol. Biol.* 157 (1) (1982) 105–132, [https://doi.org/10.1016/0022-2836\(82\)90515-0](https://doi.org/10.1016/0022-2836(82)90515-0).
- [103] H.M. Berman, J. Westbrook, Z. Feng, G. Gilliland, T.N. Bhat, H. Weissig, I. N. Shindyalov, P.E. Bourne, The protein data bank, *Nucleic Acids Res.* 28 (1) (2000) 235–242, <https://doi.org/10.1093/NAR/28.1.235>.
- [104] W. Humphrey, A. Dalke, K. Schulten, VMD: visual molecular dynamics, *J. Mol. Graph.* 14 (1) (1996) 33–38, [https://doi.org/10.1016/0263-7855\(96\)00018-5](https://doi.org/10.1016/0263-7855(96)00018-5).